Tuning the magnetic phase diagram of Ni-Mn-Ga by Cr and Co substitution

OPEN ACCESS
IOP Publishing
Journal of Physics D: Applied Physics
J. Phys. D: Appl. Phys. **55** (2022) 025002 (20pp)
https://doi.org/10.1088/1361-6463/ac2a66

Tuning the magnetic phase diagram of Ni-Mn-Ga by Cr and Co substitution

M Schröter[1], H C Herper[2] and A Grünebohm[3,*]

[1] Faculty of Physics and Center for Nanointegration Duisburg-Essen (CENIDE) Universität Duisburg-Essen, 47048 Duisburg, Germany
[2] Division of Materials Theory, Department of Physics and Astronomy Uppsala University, Uppsala, Sweden
[3] Interdisciplinary Centre for Advanced Materials Simulation (ICAMS), Ruhr-University Bochum, 44780 Bochum, Germany

E-mail: anna.gruenebohm@rub.de

Received 10 February 2021, revised 17 August 2021
Accepted for publication 27 September 2021
Published 14 October 2021

Abstract

Ni-Mn-based Heusler alloys have a high technical potential related to a large change of magnetization at the structural phase transition. These alloys show a subtle dependence of magnetic properties and structural phase stability on composition and substitution by 3d elements and although they have been extensively investigated, there are still ambiguities in the published results and their interpretation. To shed light on the large spread of reported properties, we perform a comprehensive study by means of density functional theory calculations. We focus on Cr and Co co-substitution whose benefit has been predicted previously for the expensive Ni-Mn-In-based alloy and study the more abundant iso-electronic counterpart Ni-Mn-Ga. We observe that substituting Ni partially by Co and/or Cr enhances the magnetization of the Heusler alloy and at the same time reduces the structural transition temperature. Thereby, Cr turns out to be more efficient to stabilize the ferromagnetic alignment of the Mn spins by strong antiferromagnetic interactions between Mn and Cr atoms. In a second step, we study Cr on the other sublattices and observe that an increase in the structural transition temperature is possible, but depends critically on the short-range order of Mn and Cr atoms. Based on our results, we are able to estimate composition dependent magnetic phase diagrams. In particular, we demonstrate that neither the atomic configuration with the lowest energy nor the results based on the coherent potential approximation are representative for materials with a homogeneous distribution of atoms and we also predict a simple method for fast screening of different concentrations which can be viewed as a blueprint for the study of high entropy alloys. Our results help to explain the large variation of experimentally found materials properties.

Keywords: Heusler alloys, magnetic phases, magnetocaloric, density functional theory, Mn

(Some figures may appear in colour only in the online journal)

* Author to whom any correspondence should be addressed.

1. Introduction

Magnetic Ni-Mn-(In, Ga, Sn) based Heusler alloys show a variety of complex magnetic [1–4] and structural phases [1, 5, 6], which partly transform into each other in first-order magneto-structural phase transitions. These alloys are promising in exciting applications such as spintronics, magnetic data storage, the magnetic shape memory effect, the magnetocaloric effect and thermomagnetic energy harvesting [4, 7–10]. Today, multifunctional materials which combine several magnetic properties and features are also discussed [11, 12]. Designing such materials has become feasible with the arrival of high entropy alloys [13, 14].

All applications ask for a detailed understanding and control of the magnetic structure, its stability and its coupling to structural properties. In particular, large elastic and caloric responses are possible if the external magnetic field induces the structural phase transition. In these cases, a large change of magnetization ΔM and a large shift of the structural transition temperature T_M with the field dT_M/dH are beneficial. Another key point is that T_M should be close to room temperature for many applications and a systematic way to manipulate T_M is desired. Off-stoichiometric Heusler systems and their potential for applications is a very active field with many different facets. In particular, *ab initio* calculations are frequently used to understand and optimize Heusler alloys [5, 15–19]. It has been predicted that T_M depends on the number of valence electrons per atom (e/a) and thus can be tuned by substitution with excess Mn [19–22], in accordance to experimental results for $Ni_8Mn_{1-x}Ga_x$ (with $x \leq 0.25$) [10, 18]. The trends of T_M with other substituents are still under debate. Experiments, as well as theoretical studies, show that Co substitution can work both ways and lead to an increase or decrease of T_M [23–25]. For Mn substitution by Cr, the enhancement of T_M contrary to the e/a trend has been observed in Ni-Mn-In [26], Ni_2MnGa [27, 28] and for small concentrations of Cr in Ni-Mn-Sb [29]. However, a large reduction of T_M due to Cr, i.e. the decrease of e/a has been reported for $Ni_{8-x}Cr_xMn_{7.2}Sn_{0.8}$ [30]. Recently, atomic ordering has been predicted as one of the sources of these discrepancies [31–33] and with the increasing complexity of the compounds, it became obvious that the preparation process plays a crucial role [34, 35]. So far, the investigations are restricted to small Cr concentrations (a few atomic percent) since the limited solubility of Cr hinders the investigations of larger Cr concentrations. In Ni-Mn-In [36] and in Ni-Mn-Sb it was observed that the amount of a second (unwanted) γ-phase grows with increasing Cr concentration [30].

Another important fact is that, both atomic ordering and the formation of competing phases in Heusler alloys, strongly depend on the synthesizing route and the thermal treatment [35, 37]. Recently, even the thermodynamic stability of the well-known off-stoichiometric Ni-Mn-(Ga,Sn,In) system has been refuted [38–40]. Therefore restricting the investigations to the ground state or the known phases on the Hull line does probably not allow to sample all relevant phases and atomic orderings of a real sample.

It has been shown that substitution has a large impact on the magnetic structure, in particular that compensation of ferromagnetic (FM) with antiferromagnetic (AF) interactions by substitution may enhance the change of the magnetization at T_M [41]. Furthermore, Co is often added to improve the magnetic properties in view of a larger Curie temperature or an improved hysteretic behavior, i.e. Co is viewed to reduce the hysteresis loss which denotes the energy loss in form of heat during the magnetization process [23, 42]. Here, we focus on the question of how one can optimize T_M and the magnetic structure simultaneously by co-doping with elements which favour FM (Co) or AF (Cr) phases. Having two impurities which favor opposite magnetic trends opens up a large range of possible magnetic configurations and has a potentially large magnetocaloric effect if the magnetization (M) changes at the structural transition [22, 43, 44].

So far, large changes of magnetization have been predicted by means of *ab initio* simulations for Co/Cr co-substitution in Ni-Mn-In and Ni-Mn-Sn for 5% Co/Cr substitution and specific atomic ordering in [43, 45]. A recent study [46] on Co/Ni and Cr/Mn substitution in Ni-Mn-(In,Sn) underlines the complexity of the system and poses new questions as non-linear trends between T_M and Cr-concentration have been found for particular quasi-random structures. Experimentally, a paramagnetic or AF gap below T_M has been observed in case of Cr substitution for Mn in Ni-Mn-In [26] and Ni-Mn-Sn [47].

It is worth to check the impact of Co/Cr substitution in the Ga sister compound, because compared to Sn, and particular In, Ga is cheap and far more abundant [48, 49]. Neutron diffraction revealed that Co substitution may result in a complex magnetic ordering similar to Cr substitution and AF ordering in the low temperature martensite with different ordering temperatures for the Ni and Mn sublattices have been reported [50, 51]. We note that such temperature dependent phenomena are beyond the scope of the present work. Some investigations for the Ga-based system have been made by Zagrebin *et al*. They have shown that if averaging over possible isomers is taken into account, Cr in $Ni_8Mn_2Cr_2Ga_4$ [52] leads to ferrimagnetic and FM cubic and tetragonal phases, respectively. Furthermore, they have predicted that the structural transition temperature in $Ni_2Mn_{1-x}Cr_xGa$ increases with x [53]. However, the influence of excess Mn as well as the effect of Co co-doping have to our knowledge not been studied so far. In order to close this gap, we discuss the influence of atomic structure and ordering on the relative energies of different magnetic phases in Ga-based Heusler alloys and depict concentration ranges allowing for large changes of magnetization during a structural phase transition. In particular, we discuss how replacing atoms by Cr and Co impurities affects the magnetic structure, the stability of the tetragonal phase, and the strength of the magneto-structural coupling. For functional responses, e.g. caloric response, materials with large changes in magnetization and/or structure at a given temperature are of special interest. In order to depict such systems or regions in the phase diagram, it is of eminent importance to consider also the impact of the substituents on T_M.

The paper is organized as follows: after the computational details are given in section 2, we present the impact of Cr substitution on the Ni sublattice in section 3.1 and on the Mn sublattice in section 3.2. In both cases Co impurities on the Ni sublattice have been taken into consideration. Based on the findings in sections 3.1 and 3.2 structural and magnetic phase diagrams are extrapolated and discussed in section 3.3. Conclusions and outlook are given in section 4. Detailed information on lattice constants and energy differences are summarized in the appendix.

2. Computational details

The calculations of the total energy and the atomic relaxation have been performed self-consistently with the plane wave pseudopotential code VASP [55]. Projector augmented wave potentials [56] treating Ga $4s^2 4p^1 3d^{10}$, Mn $3p^6 3d^5 4s^2$, Ni $3p^6 3d^8 4s^2$, Co $3d^8 4s^1$ [57], and Cr $3p^6 3d^5 4s^1$ states as valence have been employed in combination with the generalized gradient approximation of Perdew, Burke, and Ernzerhof [58]. For static simulations and relaxation of the ions we utilize the tetrahedron method [59] and smearing with the Methfessel-Paxton method of the electronic states of 0.1 eV, respectively, in combination with an energy cutoff of 460 eV, an energy convergence of 10^{-7} eV, and for the ionic relaxation the cutoff criterion was chosen as 10^{-5} eV. The k-mesh has been constructed with the Monkhorst-Pack scheme [60] with a $8\times8\times8$ k-points mesh. Test results for larger meshes gave changes in the range of 0.3 meV f.u.$^{-1}$, i.e. per formula unit, which corresponds to 4 atoms in the case of the Heusler alloys. Local magnetic moments were obtained by projecting the wave functions onto spherical harmonics within spheres of 1.22, 1.32, 1.06, 1.32, and 1.30 Å for Ga, Mn, Ni, Cr and Co atoms, respectively. Since consideration of non-collinear magnetic structures does not only increase the numerical effort by a multiple, but would also overlap with the relation between impurity concentration and position and the magnetic phase, we restrict our study to collinear spin arrangements.

Substitution lowers symmetry and introduces disorder through the different local arrangements of atoms. For each concentration we consider all possible short-range atomic arrangements (isomers) up to a distance of about 10 Å using simulation cells of 16 atoms, see figures 1 and 11. Note that Mn on the Y sublattice is denoted as Mn_Y while the excess Mn on the Z sublattice is named Mn_Z throughout this work. First, volume and atomic positions of the cubic phases have been optimized for each configuration and magnetic state. Subsequent static simulations are used to sample the energy landscape under tetragonal distortion [61]. Our calculations show that the energy differences between different isomers can be quite small so that it is questionable whether the most stable configuration determined for $T = 0$ K is the only relevant geometry at elevated temperatures. These small energy differences hint that all configurations may be relevant to a certain extent. Therefore, we consider not only the lowest configuration but use a homogeneous average over all possible configurations in our unit cell. We determine the energies for a homogeneous distribution of atoms on the sublattices by averaging the energies of all isomers and weighting them with the number of possible realizations in our simulation cell, see table 1. In the case of tetragonal distortions we also take the different relative alignment of the bonds and the tetragonal axis into account, see detailed discussion in section 3.3.

The obtained lattice parameters have been furthermore used to determine the pairwise magnetic exchange parameters (J_{ij}) using Liechtenstein's formula [62] as implemented in the Munich SPRKKR code [63, 64]. These calculations have been performed within the coherent potential approximation (CPA), using lattice constants which have been averaged over all isomers obtained from our VASP calculations. The calculations have been performed in the scalar relativistic mode employing the same exchange-correlation functional as for the VASP calculations. The orbital expansion was set to $l_{max} = 4$ and at

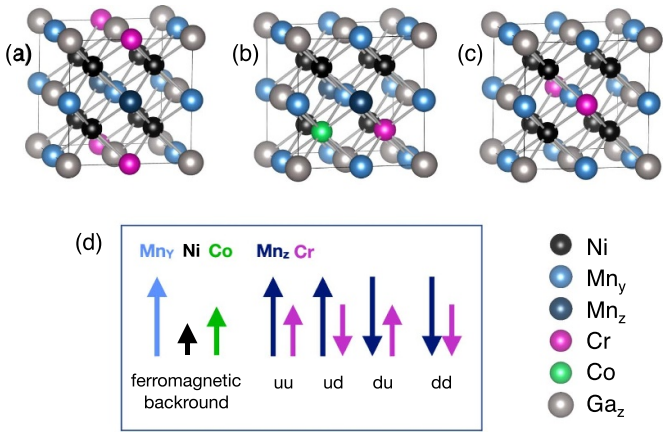

Figure 1. Exemplary simulation cells for substitution of Cr on (a) Mn (b) Ni and (c) Ga lattice and optional Co on Ni lattice (b). (a) $Ni_8Mn_4CrGa_3$: two isomers can be distinguished based on the Mn_Z-Cr arrangement either isomer (a) along [100] (shown) or isomer (b) along [111], see table 1. (b) $Ni_6CoCrMn_5Ga_3$: if two Ni atoms are replaced, the substituents may be lined up along [100] (isomer 1) shown here, [110] (isomer 2), or [111] (isomer 3), see table 1. (c) For Cr on Ga, only one isomer can be realized. (d) (Meta)-stable magnetic structures: Mn_Y, Ni and Co define the FM background [54], and up to four different magnetic variants (uu, ud, du, dd) are given by the relative alignment of Mn_Z and Cr spins. Ga is non-magnetic and not included.

Table 1. List of isomers for Cr on Ni for Ni_6 (upper panel) and Cr on Mn_Y and Ni_8 or Ni_7 (lower panel). The isomers differ in distances and directions of Co–Cr and Cr–Mn_Y neighbors, respectively, see figure 11 in the appendix for illustrations of all isomers. The last column lists the relative number of realization of the isomers used for the weighting.

System	Isomer	Bonds	Distances	Direction	Weight
Cr on Ni	1	Cr/Co-Cr/Co	$a/2$	$\langle 100 \rangle$	3[a]
	2		$a/\sqrt{2}$	$\langle 110 \rangle$	3[b]
	3		$\sqrt{3}a/2$	$\langle 111 \rangle$	1
Cr on Mn	a	Cr-Mn_Z	$a/2$	$\langle 100 \rangle$	3[a]
	b		$\sqrt{3}a/2$	$\langle 111 \rangle$	1

[a] Along tetragonal axis: 1, perpendicular: 2.
[b] 45° angle with tetragonal axis: 2; perpendicular: 1.

least 32^3 k-points were used for the derivation of the exchange parameters.

3. Discussion and results

In Ni-Mn-Ga samples, typically the Ni sublattice has a high degree of ordering while the preparation details determine whether the Mn/Ga sublattices are fully disordered (B2) or ordered ($L2_1$) [65]. If not stated otherwise, we refer to the ordered phase throughout the paper. The $L2_1$ structure of Ni_2MnGa can be understood in terms of four staggered sublattices with the full point symmetry O_h of the cubic lattice, see figure 1. Two of the sublattices are occupied by Ni (denoted as X-lattice), one sublattice is occupied by Mn atoms (denoted as Y lattice). The fourth sublattice (denoted as Z lattice) is occupied by the nonmagnetic main group element Ga. In a preparatory first step, one Ga atom is replaced by an extra Mn_z atom, assuming an otherwise perfect $L2_1$ ordering ($Ni_8Mn_5Ga_3$). Previous studies have shown that the excess Mn drives T_M closer to room temperature and that complex magnetic martensitic phases such as 14 M can be avoided, see phase diagram in reference [66]. It has been further discussed in literature that Co tends to occupy Ni positions [31, 67, 68] whereas different Cr positions may be possible depending on processing conditions [44, 69]. The framework for our investigation are the three alloys $Ni_{8-x_1-x_2}Co_{x_1}Cr_{x_2}Mn_5Ga_3$ (section 3.1), $Ni_{8-x_1}Co_{x_1}Mn_{5-y}Cr_yGa_3$ and $Ni_{8-x_1}Co_{x_1}Mn_{5-y}Cr_zGa_3$ (section 3.2).

The relevant magnetic structures are summarized in figure 1(d): the spins of Ni, Co, and Mn_Y atoms are always aligned in parallel and define the FM background of the alloy while the Ga atoms are basically non-magnetic and can be neglected. Against this background, the magnetic alignment of Mn_z and Cr define up to four (meta)-stable magnetic variants uu, ud, du, dd. Here we use the nomenclature u (d) for FM (AF) aligned spins where the first character corresponds to the orientation of the Mn_Z spin relative to the FM background.

For ordered $Ni_8Mn_5Ga_3$, we find the tetragonal phase with $c/a = 1.3$ to be 75 meV f.u.$^{-1}$ lower in energy than the cubic phase. As discussed in literature the cubic phase is stabilized at high temperatures by entropy and this energy difference, translated via $\Delta E = Nk_BT_E$, with N being the number of atoms, and the Boltzmann constant k_B, gives a rough estimate of the transition temperature T_M [15]. Using this approximation for $Ni_8Mn_5Ga_3$ we obtain a transition temperature of about 218 K which is in fairly good agreement with the findings by Gruner *et al* [15]. Deviations in absolute values may arise from different structure optimization techniques. In both phases, the d configuration is lower in energy than the u alignment of all spins in accordance with previous experimental and theoretical findings [31, 70]. This can be understood in terms of the AF coupling between Mn_y and Mn_z nearest neighbours, see blue diamonds in figure 2.

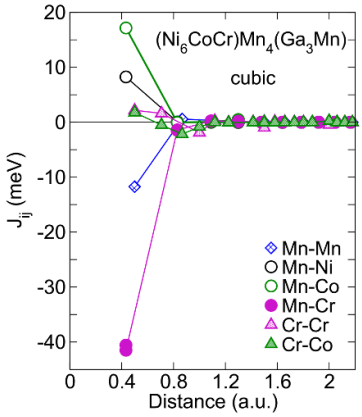

Figure 2. Representative pair-wise magnetic exchange parameters for $(Ni_6Cr_1Co_1)Mn_4(Ga_3Mn)$ (cubic, ud order) for a homogeneous distribution of Ni, Co and Cr atoms on X lattice and excess Mn on Z lattice. Negligibly small J_{ij} between Mn atoms on the same sublattice and interactions with Ga atoms as well as the Cr–Ni interaction which is about 1 meV for the nearest neighbour interaction are omitted.

3.1. $Ni_{8-x_1-x_2}Cr_{x_1}Co_{x_2}Mn_5Ga_3$: substituting Cr and Co for Ni

Starting from ordered $Ni_8Mn_5Ga_3$, we replace up to two Ni atoms with Cr_x or Co_x ($x = 1, 2$). In all cases, the magnetic moments depend only weakly on the structure and the Co and Cr spins are parallel and antiparallel to the background for all configurations. Thus, two different magnetic phases with FM Mn_Z (u) and AF Mn_Z (d) can be distinguished. Before we discuss the systematic trends with substitution, it is important to understand the impact of atomic ordering on the material properties. For convenience we first focus on disorder effects among magnetic ions, i.e. Mn–Cr or Mn–Co, and discuss the minor influence of Mn-Ga ordering afterwards.

For $x = 1$ the atoms on the X-lattice have one Mn_Z and four Mn_Y nearest neighbours along the space diagonals with a distance of $\sqrt{3}a/4$, see figure 1(b). If two Ni atoms are replaced, three different nearest-neighbour configurations (isomers) can be realized, which are characterized by the spatial relationship of both substituting atoms, see table 1. In the latter cases one furthermore may distinguish tetragonal strain along or perpendicular to the connection line of both substituents. By way of example, the energy variation with tetragonal distortion of Cr_1Co_1 is illustrated in figure 3(a) and all energy curves are provided in figure 12. For all cases, we find isomer 1 to be lowest in energy. This isomer is also lowest in symmetry and thus the largest atomic relaxations occur. However, the energy differences between isomers in the cubic phase are usually not exceeding 25 meV f.u.$^{-1}$ [71], i.e. an energy difference which is rarely relevant for the ordering of atoms during the sample preparation at several hundreds Kelvin. The energy curve of the most favourable configuration, isomer 1 with the Cr–Co bond along the tetragonal axis, deviates considerably from the mean energies for a homogeneous distribution of atoms (shaded areas) marked as separate lines in figure 3(a), but has

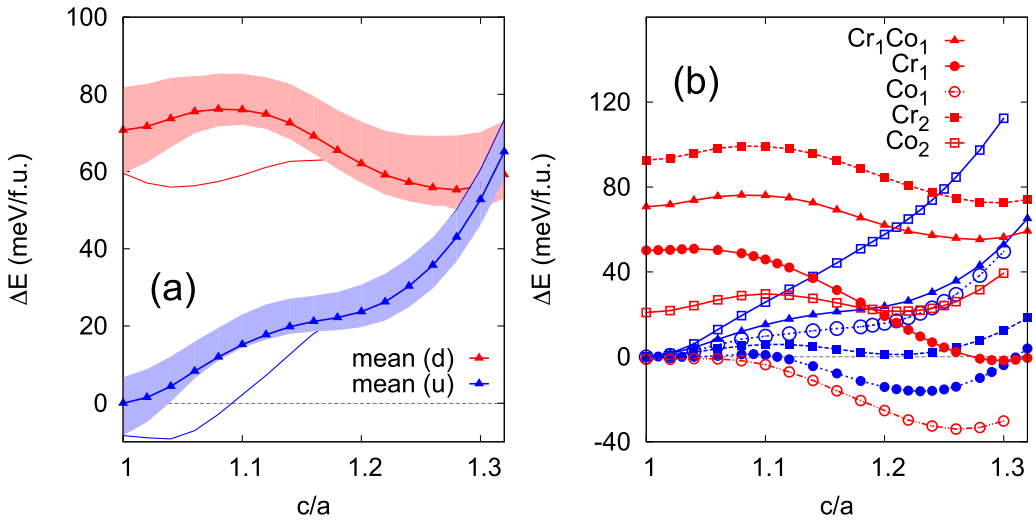

Figure 3. Energy variation (ΔE) with tetragonal distortion relative to the u state at $c/a = 1$ for $Ni_{8-x_1-x_2}Co_{x_1}Cr_{x_2}Mn_5Ga_3$. Colours encode the magnetic state of Mn_Z u (blue) and d (red) and symbols encode stoichiometry: triangles: $x_1 = x_2 = 1$, circles: $x_1 = 0$, $x_2 = 1$ (filled) $x_1 = 1$, $x_2 = 0$ (open) , squares: $x_1 = 0$, $x_2 = 2$ (filled), squares: $x_1 = 2$, $x_2 = 0$ (open). (a) Variation of ΔE with distribution of substituents for the example $x_1 = x_2 = 1$, see curves for all configurations in appendix figure 12. Shaded areas: range of energies for all but one configurations and thin lines the only configuration showing a different trend with c/a (isomer 1, both substituents aligned parallel to the tetragonal axis). Mean energies are added as lines with symbols and are summarized for all stoichiometries in (b).

a low impact due to its low probability of realization (1:7), see table 1. Except for the single outlier with the bond along the tetragonal axis, the overall trend, i.e. shape of the c/a variation and energy differences, shows a similar behaviour for all cases despite different Co-Cr distances, see table 1. Considering the limited solubility of Cr in these systems [36], larger Cr concentrations have been excluded from our study.

Figure 3(b) summarizes the results for different concentrations of Co/Cr substituents for a homogeneous distribution. In the cubic phase, Cr and/or Co impurities in the Ni sub-lattice tend to stabilize the FM alignment of the Mn_z atoms and thus lead to an increase of the magnetization. Hereby, Cr is more efficient in stabilizing the FM Mn_Y-Mn_Z configuration, as can be seen in the ordering of ΔE. For one Co atom, u and d states are of the same energy in agreement to previous work [72], but ΔE increases to about 21, 50, 71, and 92 meV f.u.$^{-1}$ for Co_2, Cr_1, Cr_1/Co_1, and Cr_2, respectively. In the u state, the magnetization is larger in case of Co substitution as each Ni moment (0.3–0.4 μ_B) is replaced by a moment of about 1.0 μ_B/atom and of about -2 μ_B for Co and Cr substitution, respectively.

The underlying mechanism for the stabilization of the u phase by Cr and Co is different, as can be understood by means of the magnetic exchange interactions, see figure 2. On the one hand, Co adds FM couplings by the direct FM Co–Mn exchange (green circles), exceeding the FM Ni–Mn exchange (open black circles) roughly by a factor of two. Though the size of the Co–Mn coupling does not change within our concentration range, the number of couplings does. That means with increasing amount of Co, the FM alignment of Mn spins becomes slightly more favourable, for a detailed discussion see section 3.2. On the other hand, Cr induces large AF Cr-Mn couplings (filled purple circles), which exceed the Mn_Y-Mn_Z (blue diamonds) couplings roughly by a factor of four. Already for one Cr-atom in the simulation cell, five Cr-Mn pairs (compared to 4 Mn_Y-Mn_Z) exist and thus the AF Mn_Y-Mn_Z interaction is frustrated and Mn spins align parallel to each other to optimize their alignment with Cr.

If one of eight Ni atoms is substituted, the mean energetic ground state is tetragonal with $T_E \approx 46$ K and $T_E \approx 96$ K for Cr and Co substitution, respectively. These trends of the structural transition temperature qualitatively agree with experimental findings for $Ni_{8-x}Co_xMn_5Ga_3$ [23], showing a significant decrease of T_E with x ($x = 0$: 376 K and $x = 1.1$: 182 K). The larger reduction of T_E with Cr is in line with the larger reduction of the number of electrons per atom (e/a) with Cr rather than Co substitution. Indeed, for one Cr the value of $e/a = 7.5$ corresponds to the value of Ni_2MnGa, for which a similar T_E of about 90 K has been predicted [66]. For two out of eight substituents, the cubic phase with Mn u always is the global minimum of the mean energy, while remnants of the tetragonal minima around $c/a = 1.2$ at lower level of substitution can only be found as extrema of higher order. For pure Co substitution, we observe the systematic trend in accordance with e/a when going to 2 dopants.

Importantly, the distribution of atoms plays an equally important role for the relative energies of cubic and tetragonal phases. Thus, states with low but finite T_E, shown for $x_1 + x_2 = 2$ in figure 4, occur for single orientations of ordered isomers, e.g. in case of $x_1 = x_2 = 1$ (one Co and one Cr impurity), only the configuration isomer 1 with both substituents aligned along the tetragonal axis has a small tetragonal minimum at $c/a = 1.04$. The same holds for the case of two Co impurities. This effect averages out assuming that in a real sample all configurations exist to a certain extent. The impact of atomic ordering is even more important for the case of two Cr atoms. In this case, all three isomers show a tetragonal minimum for specific directions of the tetragonal axis which would result in a finite T_E, see figure 4. But again, their

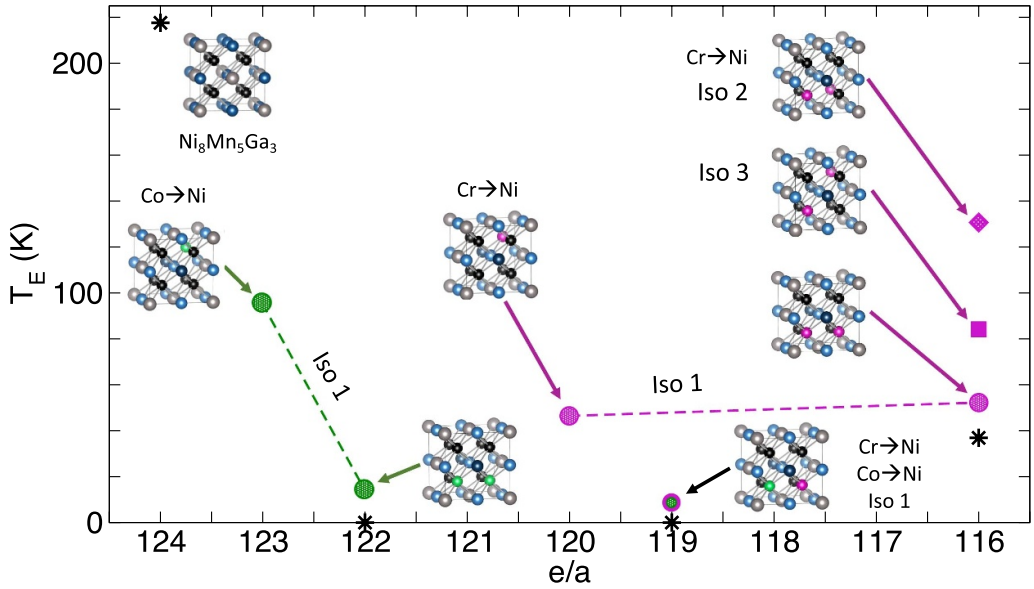

Figure 4. Qualitative trends of energy difference between cubic and tetragonal states translated to thermal energy (T_E) with Co/Cr substitution for Ni, as illustrated in green/magenta. Here, only the most favourable magnetic states have been taken into account. Stars mark the T_E obtained from the homogeneous solutions which consider all isomers including their weights, and circles, diamonds and squares illustrate results for isomers 1, 2 and 3 showing always the configuration with the largest T_E, see table 2. With this it becomes obvious that the tetragonal phase vanishes for $x_1 + x_2 > 1$.

weight is not sufficient to keep the minimum for a random distribution of substituents and more than one impurity on the Ni lattice destroys the phase transition unless the method of synthesis favours specific isomers, in this case isomer 2 with Cr–Cr bonds along the tetragonal axis as well as isomer 3. With an experimental method which allows for a selective synthesis, the system with Cr impurities bears the potential for a reasonable T_E.

To summarize, replacing Ni by Cr and/or Co reduces e/a and T_E drops to lower temperatures or vanishes completely, as is commonly expected. This is in full agreement to previous observations on $Ni_{50}Mn_{37}In_{13}$ where Cr on Ni reduces T_M and, except for very small impurity concentrations, this substitution reduces the total entropy change at the structural transition temperature T_M [69]. However, this holds only if we average over all possible isomers and orientations. In all cases, impurities reduce e/a compared to $Ni_8Mn_5Ga_3$, but though the e/a for $Ni_7CrMn_5Ga_3$ is larger then for $Ni_6Cr_2Mn_5Ga_3$, the latter has configurations with significantly higher T_E, see figure 4. One possible explanation could be that structural changes depend not only on the electronic structure, but also on the magnetic interactions. Especially the strong Mn–Cr interaction might play a role here.

3.2. $Ni_{8-x_1}Co_{x_1}Mn_{5-y}Cr_yGa_3$: substituting Cr for Mn and Co for Ni

As shown in the previous section, substituting Ni by Cr either reduces T_E significantly or the tetragonal ground state vanishes completely already for a moderate concentration of substituents. In the next step, Cr impurities occupying the other sublattices are investigated in order to understand the impact of Cr–Mn and Mn–Mn distances on the structural and magnetic properties. Experimentally, Sharma *et al* found an increase of the structural phase transition temperature, an increase of AF couplings and the change of the magnetic moment at T_E, if Cr replaces Mn in the In-based alloy [44]. They argue that the smaller size of Cr will cause a positive pressure in the system and thus reduce the Mn–Mn distances, which results in such preferable properties. Because our Ga-Heusler alloy is iso-electronic to the In system, we test whether a similar improvement is possible and whether the assumed mechanism is still valid if the smaller Ga is used instead of In.

In the following we discuss the stoichiometry $Ni_{8-x}Co_xMn_4CrGa_3$. Replacing Mn for Cr, leaves us with two possible scenarios, since Cr can occupy a regular Mn site (Y lattice) or replace the excess Mn on the Z lattice. In our simulation cell this can be realized with two Cr_Y isomers and one Cr_Z configuration, see figure 1 and table 1. Figure 5(a) illustrates the mean energy curves (lines with symbols) and the range of energies for different isomers (shaded areas) for Mn_Y while figure 5(b) shows the single realization for Mn_Z. In analogy to the discussion in the previous section, we construct the mean energy by averaging over the energies of all structures weighted with their probabilities, see table 1. For Cr_Y all four possible magnetic states (dd: 1.2 μ_B f.u.$^{-1}$, du 3.0 μ_B f.u.$^{-1}$, ud 3.4 μ_B f.u.$^{-1}$ and uu with 5.1 μ_B f.u.$^{-1}$) are at least metastable and Cr_Z spins may align u and d. For the cubic phase the energy differences of all spin structures are below 25 meV f.u.$^{-1}$ for Cr_Y, while the anti-parallel alignment of Cr_Z is about 60 meV f.u.$^{-1}$ more favourable. Under tetragonal distortion, the energy differences between the magnetic phases increase. For a fixed stoichiometry, the tetragonal Cr_Z d phase is lowest in energy and the tetragonal du phase is the most favourable Cr_Y phase.

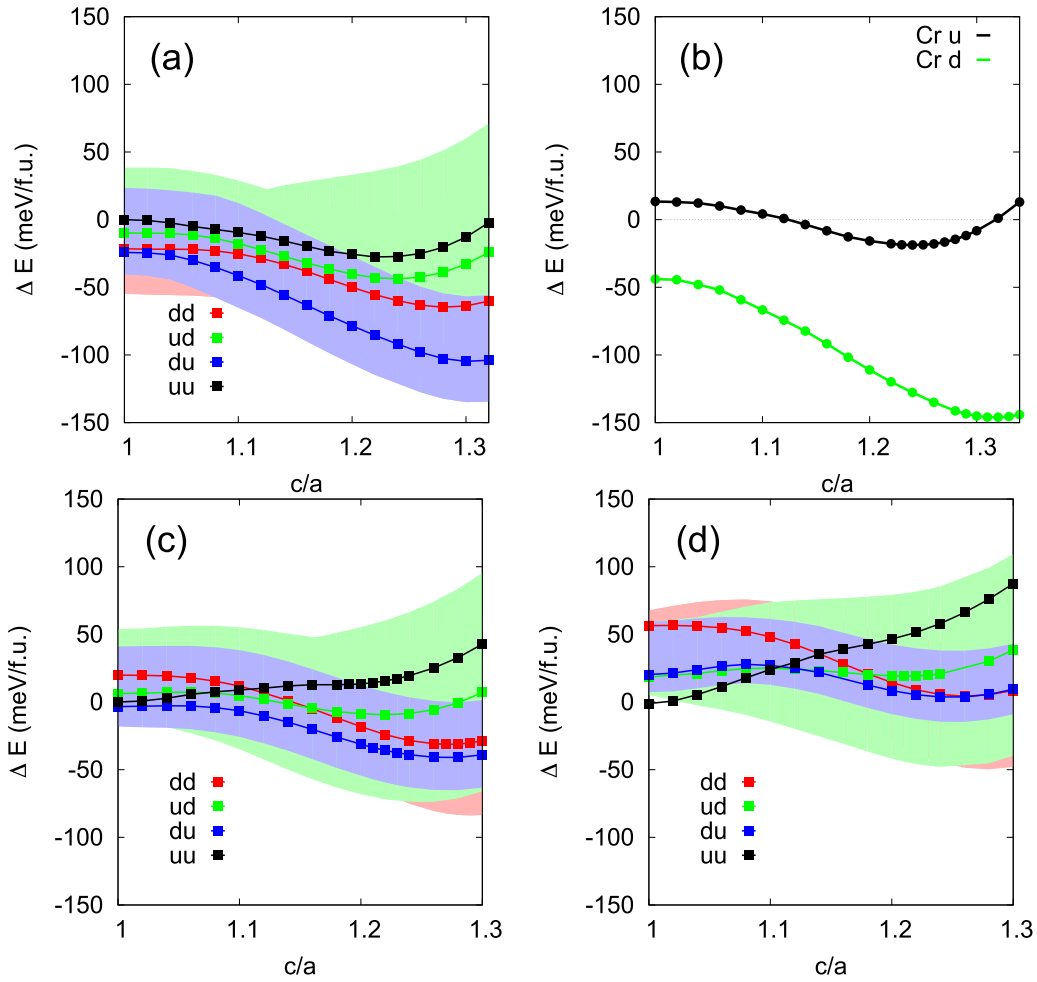

Figure 5. Energy variation with tetragonal distortion for $Ni_{8-x}Co_xMn_4CrGa_3$ for (a) Cr_Y and (b) Cr_Z relative to the energy of the cubic uu phase for Cr_Y. (c)–(d) Impact of Co_X co-substitution for Mn_Y (c) $x = 1$, (d) $x = 2$. For Cr_Y different Cr–Mn orderings have been considered (cf figure 13) and lines with symbols illustrate mean energies for a homogeneous distribution of atoms and for ud, du and dd the spread of energies of these different isomers is added to the figures by shaded regions.

The stability of the different magnetic states can be understood by means of the magnetic exchange interactions shown in figure 6. In case of Cr_Z no nearest Mn_Y-Mn_Z neighbours exist, thus FM Ni-Mn and AF Mn-Cr interactions dominate the magnetic phase and stabilize the Cr d state [73]. For Cr_Y, the du state is particularly favourable due to the three AF Mn_Y-Mn_Z interactions and the strong Cr-Mn_Z interaction. However, as there is only one Cr-Mn_Z pair in the system and the AF Mn_Y-Cr interaction is almost vanishing, the dd phase is only about 7 meV f.u.$^{-1}$ less favourable.

The interactions also allow us to deduce some qualitative trends of the Mn-Ga-Cr ordering, see subfigures (a)–(c). With increasing disorder (going from Cr_Z to Cr_Y to B2 order), the number of possible magnetic configurations and relevant magnetic interactions and their frustration increases. Thus going from Cr_Z to Cr_Y; (1) The number of possible magnetic states in the simulation cell increases from two to four; (2) The overall AF interaction increases (Cr–Mn increases by -2 meV and additional Mn_Y-Mn_Z interactions of -8 meV occur); and (3) Additional frustration is induced by AF Cr-Cr and Mn_Y-Cr interactions. In turn, the energy difference between the magnetic phases decreases with increasing disorder, a trend which may be even more pronounced for complete Cr-Mn-Ga disorder where further large AF Cr_Y-Cr_Z interactions occur (see figure 5(b)).

For all distributions of Cr, the Mn-Mn and Mn-Cr interactions between different sublattices increase in the x–y plane and dominate the tetragonal phase, although the interactions along z-axis become FM with tetragonal distortion. One may speculate that the reduction of T_E with increasing disorder, i.e. going from Cr_Z to Cr_Y and probably to B2, may be related to the increasing frustration, as more and more AF interactions occur already in the cubic phase (figures 6(a)–(c)) and are even stronger in the tetragonal phase (figures 6(c) and (e)).

As discussed in section 3.1, additional Co impurities on the Ni lattice are taken into account since this element will most likely be added in experimental realizations to avoid hysteresis losses and other effects which reduce the magnetic performance in such Heusler alloys at finite temperatures [42]. In the following, we discuss the influence of additional doping with Co_X using the stoichiometry $Ni_7CoMn_4CrGa_3$ as example, see figure 1. In case of Cr_Z, one may expect that Co_X substitution successively stabilizes the u phase, however, due to the rather large energy difference between both phases, we expect that

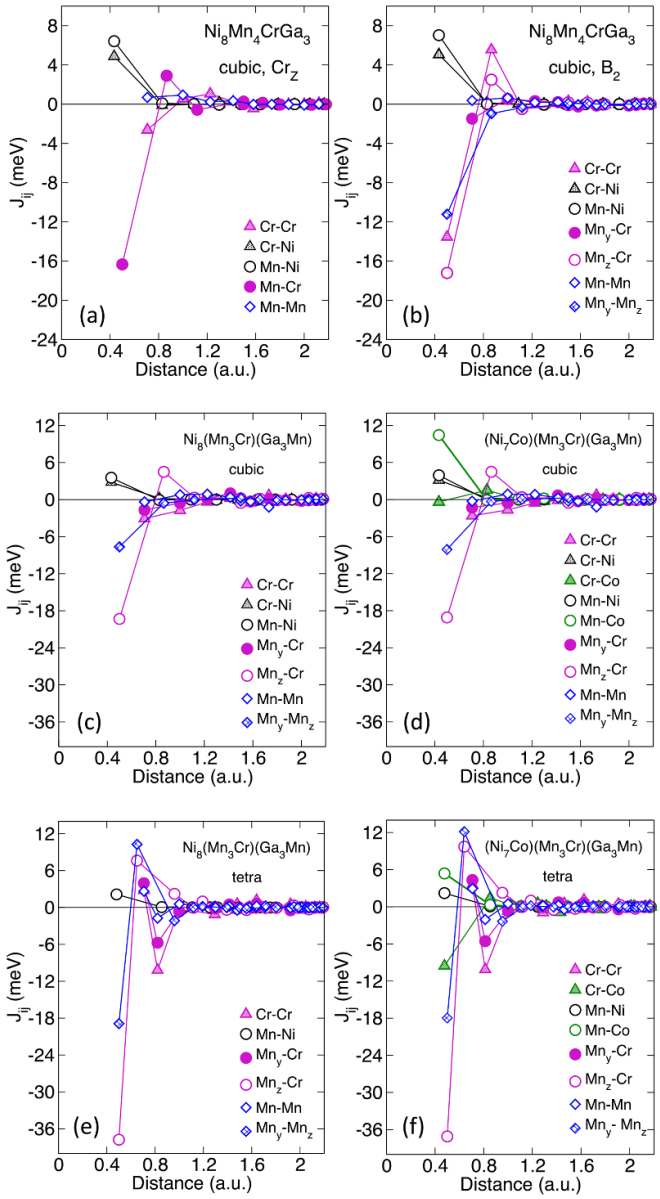

Figure 6. (a)–(c): impact of Cr-Mn order on the pair-wise magnetic exchange parameters for cubic $Ni_8Mn_4CrGa_3$ (a) Cr_Z, (b) homogeneous distribution of Mn/Cr/Ga on Y and Z sublattice (B2 order) and (c) Cr_Y. (e)–(f): impact of tetragonal distortion (d),(f) (cf (c)/(e) and (d)/(e)) and Co substitution (cf (c)/(d) and (e)/(f)) for Cr on Y lattice. All Ni-Ni, Co-Co, Co-Ni and Ga-related exchange coefficients are smaller than 1 meV and not shown in the figure. The same holds for the Cr-Ni couplings of the tetragonal phases in (e) and (f). Note that the calculations have been carried out using CPA, i.e. the impurity atoms are homogeneously distributed on the corresponding sublattices denoted by the brackets in figure (c)–(f), using different magnetic reference structures (a)–(b) uu and (c)–(f) du, and the plot ranges differ.

larger Co concentrations are needed to stabilize the u state, but which are most likely not showing any tetragonal distortion anymore. Therefore, we restrict the discussion to the complex magnetic phases of Cr_Y. For Co_1, one of the nearest Ni-Cr neighbours is replaced and all possible Co sites of isomers (a) and (b) have the same symmetry. In the case of two Co atoms, we reduce the large configurational space of possible isomers and consider only the Co-Co distribution with the highest symmetry (isomer 3 in the last section) for isomers (a) and (b). This is justified by the small impact of the Co–Co distribution on the energies and the magnetic phases discussed in the previous section, see also figure 12.

Adding one Co_X atom to the Cr_Y system does not alter the most favourable magnetic state for any value of c/a (du state). However, for the cubic phase uu and du are nearly degenerated and at the tetragonal minimum the dd phase becomes low in energy, see figure 5(c). These trends continue with increasing Co concentration, as the uu phase is now most favourable for the cubic structure for Co_2 while du and dd are degenerate and correspond to the local energy minimum, around $c/a \approx 1.25$ in this case. Thus, with an increasing amount of Co, the preference for parallel spin alignments (dd, uu) between Cr and excess Mn grows successively. To understand the role of Co impurities on the magnetic properties, we compare the exchange parameters J_{ij} for the Co free system $Ni_8Mn_4CrGa_3$ (figures 6(c) and (e)) to the system with 1 (cf (d) and (f)) and 2 (not shown) of all Ni atoms replaced by Co. First, the Mn_Y-Mn_Z and Cr_Y-Mn_Z interactions are barely modified by Co addition, making the du and dd phases the most favourable cubic state for low Co concentrations. Second, the discussed increase of the overall AF interactions in the tetragonal phase is independent from the Co concentration (compare figures 6(c) and (e) with (d) and (f)). Considering the existence of a plethora of magnetic phases, isomers, and competing interactions, a frustrated magnetism at low temperatures seems very likely. Third, Co successively stabilizes the cubic uu phase by a FM coupling between Co and Mn of about +10.4 meV. Fourth, the Cr–Co interaction is negligible in the cubic phase, but induces additional AF interactions under tetragonal strain, thus stabilizing the dd state with an increasing number of Co atoms.

Similar trends have been found for $Ni_{7.2}Co_{0.8}Mn_{5.9}In_{2.1}$ [43]. However, a slightly higher Co–Mn coupling (18 meV) as well as FM and negligible Co–Cr couplings for cubic and tetragonal state, respectively, stabilize the uu/dd^t states already for a smaller Co concentration in the In system. These differences could partially be related to the smaller volume in the Ga case, but one should also note that the ratio of Mn/Ga atoms is different which may considerably modify the couplings. In particular the missing additional FM couplings and the fact that the Co–Mn couplings in the cubic phases are about 20% smaller in the Ga system compared to the In system (see [43]), might hinder the increase of T_C which is otherwise observed for Co impurities.

Importantly, the impact of atomic ordering on magnetic exchange interactions and energy differences between magnetic and structural phases underlines the failure of the simple discussion of T_E in terms of the number of electrons per atom. Although there is some arbitrariness in the definition of T_E the results show that the stability of the tetragonal phase is strongly correlated with Cr-Mn and Mn-Mn distances in the system, depending not only on the stoichiometry but also on the atomic ordering. Taking the case of $Ni_8CrMn_4Ga_3$, where a single Mn atom has been replaced by Cr, there it comes with

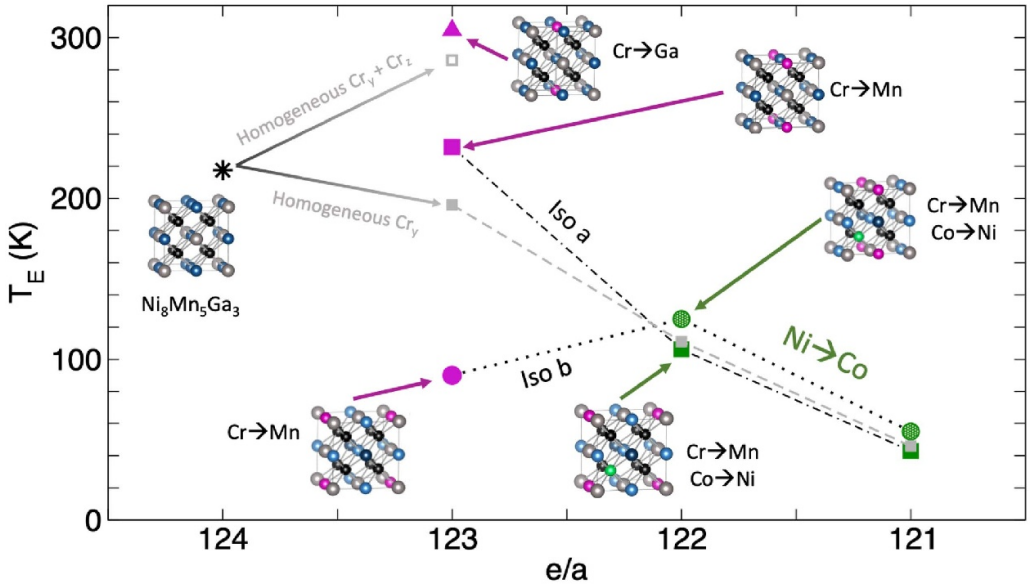

Figure 7. Qualitative trends of T_E for $Ni_{8-x}Co_xMn_4CrGa_3$. Squares (circles) denote T_E for isomer a (b) while the triangle marks the transition temperature for Cr_Z and green and magenta illustrate substitution of Ni by Co and of Mn by Cr. The homogeneous solution includes all isomers for Cr on the Mn lattice taking their weight into account. For $x_1 = 0$ also the T_E including a Cr distribution on Y and Z ($Cr_Z + Cr_Y$) is shown. In the latter case the addition of Cr leads actually to an increase in T_E. With the exception of isomer b for Co_1, Co always tends to decrease T_E. The fully homogeneous distribution $Cr_Y + Cr_Z$ for $Ni_8Mn4CrGa_3$ added by an open gray square, was obtained from $T_E = (3 * \Delta E(\text{iso a}) + \Delta E(\text{iso b}) + 4 * \Delta E(Cr_Z))/7$.

a plethora of possible configurations which all lead to different T_E. For Cr on the Mn sublattice, T_E would increase by about 55 K compared to the Cr free-case $Ni_8Mn_5Ga_3$ for isomer (a), while a realization of isomer (b) would reduce the temperature to only 90 K [74]. As discussed before in experiment, depending on the synthesis or growth process, it is very likely that both isomers occur, i.e. Cr is homogeneously distributed on the Y lattice, which would lead to $T_E = 196$ K (including the different weight of isomer a and b). So the temperature seems to decrease slightly with e/a. However, taking into account that Cr could replace Mn on the Z lattice, changes the picture. Cr on the Z lattice stabilizes the tetragonal phase and would push T_E to 305 K. Including this in the homogeneous average, T_E increases to 286 K, see figure 7. This is in contrast to the common trend of T_E increasing with e/a but agrees with experimental observations for Cr substituting Mn in $Ni_{50}Mn_{33.66}Cr_{0.34}In_{16}$ [44]. It thus becomes obvious that looking at a single isomer or a single orientation in theoretical investigations can again be misleading. Though isomer (a) follows the trend of the homogeneous average, isomer (b) shows a slight increase of T_E in case of Co_1 [75], however since this configuration has a low weight it does not influence the overall trend.

Despite the fact that the exact values of T_E depend on which configurations are considered and whether we average over different configurations, the calculations reveal trends in T_E depending on the impurity atoms, see figure 7. Cr has the tendency to increase the transition temperature, whereas adding additional Co on the Ni lattice results in the reduction of T_E, i.e. the same trends as discussed in section 3.1, see figure 7. A destabilization of the tetragonal phase is observed for all configurations in both isomers with T_E. If 12.5% of the Ni atoms have been replaced by Co, T_E decreases to 111 K for a homogeneous distribution of Cr on the Y lattice (Cr on Ga has not been considered in combination with Co impurities) and almost vanishes for 25% of Co.

In agreement with the experimental findings by Sharma [44], we find stable T_E for substitution of Mn by Cr and an increase of the overall AF coupling. Sharma *et al* conclude that the changing Mn-Mn distances due to Cr outweighs the electronic effect due to the decreasing number of valence electrons. However, in our system, the overall lattice constant is rarely modified for small concentrations of Cr on the Y lattice, i.e. Cr only acts as internal pressure if (partly) sitting on the Z lattice, see tables of 2 and 3. Internal pressure is thus less important than predicted in the case of In, possibly because the Ga ion is more similar in size to the transition metals than In. However, our calculations reveal that the number of Cr-Mn and Mn-Mn pairs is the determining factor for T_E in the Ga alloy whereby the Cr-Mn interactions are as important as the pure Mn couplings.

In summary, substitution of Cr for Mn allows to modify the magnetic structure of the alloy while keeping a proper T_E for applications and might allow to stabilize a large jump of the magnetization from an AF tetragonal phase to FM (uu) cubic phase. But, AF couplings are still present in the cubic phase and depending on atomic ordering (isomers) ud or dd are more stable.

3.3. Phase diagrams

In order to maximize the change of the magnetization at T_E and at the same time keeping T_E large and avoiding the miscible limit for the case of Cr asks for fine tuning the concentration of

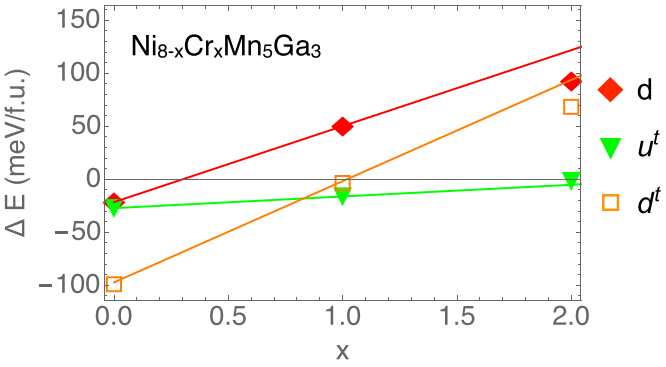

Figure 8. Exemplary illustration of the construction of phase diagrams for Cr substitution on the Ni lattice. The energy of the cubic u phase is used as reference and the energy differences for cubic d (red), and tetragonal u (green) and down (orange) states are shown for varying Cr concentration x by symbols. Linear extrapolation between $x = 0$ and $x = 1$ is used to determine the most favourable magnetic/structural phase for intermediate Cr concentrations.

dopants. It turned out that the determination of the energy differences between the magnetic phases in doped Heusler system is quite challenging for smaller Co/Cr concentrations. The CPA approach would usually be the preferred choice to study small changes in the concentration of dopants. However, it has been shown, e.g. in reference [25], and confirmed by test calculations within the present work, that the energy differences between magnetic phases are not well described by this approach due to missing atomic relaxation and the impact of the short-range structure. In order to avoid computationally heavy simulations of different isomers in larger supercells, we instead use the energies found for the chosen system size in combination with linear interpolation to construct approximate phase diagrams for the homogeneous distribution of atoms on the sublattice and for specific isomers. Thereby, we focus separately on cubic and tetragonal states. For those configurations, where the energy does not show a minimum for $c/a > 1$, we use higher order extrema which are still present in our data as remainders of the local minima of the Co/Cr free parent system.

Figure 8 illustrates the linear interpolation for the example of Cr_X substitution and a collection of all interpolations can be found in the appendix (figures 14 and 15). We use the cubic u state as reference and plot the energy differences for cubic d (red) and tetragonal u (green) and down (orange) states. As mentioned before, the Cr spins are always aligned AF to the FM background in case of substitution for Ni. Without Cr ($x = 0$) the magnetic d states are most favourable. However, their energies increase relative to the reference state with x, and for $x \approx 0.2$ and 0.8 we observe a transition to the u states being lower in energy for the cubic and tetragonal phase, respectively. It is important to note that this is a rather rough estimate, only meant to narrow down interesting concentration ranges for further studies. We do not expect any quantitative predictive power from such a simple approximation. For example, extending the interpolation to the range between $x = 0$ and $x = 2$ would change the stability range by about 0.2 for the Cr case. Fortunately, the linear interpolation between two data points also yields a good estimate of the third data point if available in case of Co substitution.

The resulting approximate phase diagrams for $Ni_{8-y}Cr_xCo_yMn_{5-x}Cr_xGa_3$ are shown in figure 9. There, black stars mark concentrations for which explicit simulations have been performed and background colours indicate the magnetic phase with the lowest interpolated energy. Without Cr and/or Co impurities, the cubic structure favours the d phase with a magnetic moment of 3.1 μ_B. With the substitution of Ni by Cr and Co, the Mn u state becomes favourable, see figure 9(a). As discussed based on the magnetic interactions, more than 1 Co atom is needed to stabilize the FM state while 0.2 Cr are sufficient. Figure 9(b) illustrates which state is most favourable at $T = 0$ K within our simulations. The tetragonal state is no longer stable for large Co/Cr concentrations, and the stability range of the d phase is larger in the tetragonal than in the cubic state. Finally, these two diagrams are superimposed in figure 9(c). For area (I) and (I^b), a structural transition at finite temperatures can be expected, however both phases share the same magnetic ground state, i.e. the change in magnetization between both structures is smaller than 0.6 μ_B f.u.$^{-1}$ In area (II) the largest changes in magnetization are likely, since here a transition from cubic u to tetragonal d is favourable and for all investigated systems the difference of the total moment between the d and u solution is about 2 μ_B f.u.$^{-1}$ In area (III), i.e. large Cr and Co concentrations, the ground state at $T = 0$ K is already cubic. Unfortunately, region (II) is restricted to a small range of Cr concentrations, challenging its experimental realization. Although the magnetic states are less sensitive to the Co concentration, T_E is drastically reduced and thus also the Co concentration needs to be adjusted carefully.

In the same way, the phase diagrams for Co_X and a homogeneous distribution of Cr on the Y-lattice are illustrated in figures 10(a)–(c). It has to be noted that one cannot distinguish between Cr u and d states without Cr and thus the choice of the ground state for small Cr concentration is not well defined. For the cubic structure (figure 10(a)), the du and uu phases are most favourable for Co concentrations below and above 1, respectively. The ground state at $T = 0$ K is given in figure 10(b). For concentrations below the line $Co_{1.5}Cr_0$–Co_2Cr_1, the tetragonal du^t phase is found to be stable whereas no phase transition is likely for higher concentrations of substituents. Extrapolation to higher Cr concentrations (not shown) hints to a change from du to ud phase in agreement to the findings for $Ni_8Mn_2Cr_2Ga_4$ by Zagrebin *et al* [52]. This is plausible considering the fact that Mn_Y-Mn_Z and Cr-Mn pairs stabilize AF Mn_Z or AF Cr alignment, respectively, and their number decrease and increase with Cr concentration. Finally, the combined diagram in figure 10(c) allows to distinguish three different regions: in region (I), i.e. for low Co concentration, a structural phase transition within the du state is the most likely scenario ($\Delta M \approx 0.3\mu_B$ f.u.$^{-1}$). In region (II) the magnetic ground state changes from uu to du^t during the structural transition ($\Delta M \approx 2.5\mu_B$ f.u.$^{-1}$), and in region (III), i.e. for high Co concentration, the phase transition is unlikely. Thus, the largest jump of the magnetization and largest T_E can be

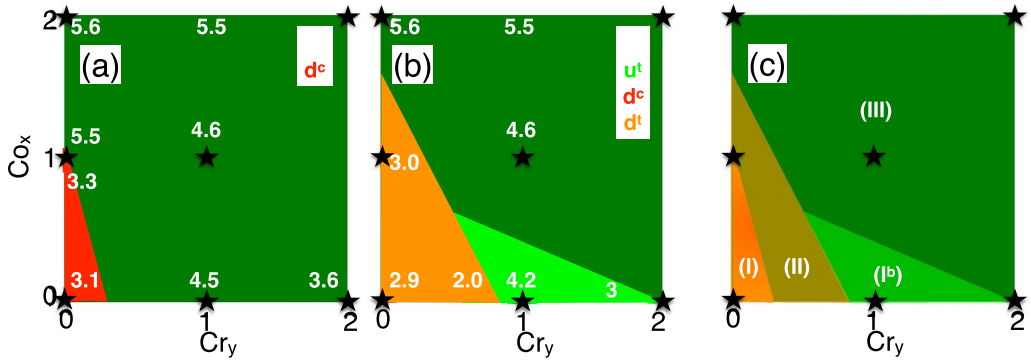

Figure 9. Estimated phase diagrams for $Ni_{8-x-y}Cr_xCo_yMn_5Ga_3$ based on VASP simulations. (a) Magnetic ground state of the cubic phase; (b) structural and magnetic ground state at $T = 0$ K; (c) combined phase diagram: (I) denotes structural phase transitions with small change of M (I: d^c-d^t, I^b: u^c-u^t), (II) stands for structural phase transition with large change of M and (III) marks regions with no phase transition. Note that the legends show only the relative orientation of Mn_Z spins, Cr is always d and not added in the notation.

expected for Co concentrations slightly above 1 in combination with a finite substitution of Cr for Mn.

The stability of magnetic phases is rather insensitive to small changes of Co/Cr concentrations. However the phase diagram changes drastically if we assume that a specific atomic ordering could be stabilized, as shown for the isomer and tetragonal direction with lowest energy in figures 10(d)–(f). In this case, the favourable cubic phase for large Cr and small Co concentrations is dd with the smallest magnetic moment of 1.2 μ_B f.u.$^{-1}$, see figure 10(d). Furthermore, a finite T_E is possible in the whole Co/Cr concentration range and for large concentrations of Cr and Co the ud^t phase is lower in energy rather than the du^t phase found for smaller concentrations of dopants or in case of the homogeneous distribution, cf subfigure (e). In turn also the combined phase diagram for this specific atomic distribution differs considerably from its counterpart for homogeneous distributions, see subfigures (c) and (f). The concentration range (I) with du^c to du^t transition is reduced and one may depict region (I^a) with a slightly larger change of $M \approx 0.5\mu_B$ f.u.$^{-1}$, given by a du^c to ud^t transition. Furthermore, for high Co and Cr concentrations (range II^a) the potential jump of magnetization is reduced from 2.5 μ_B f.u.$^{-1}$ to 1.8 μ_B f.u.$^{-1}$ for uu to ud^t transition and in the lower right corner of the diagram (region II^b) we find a dd to du^t transition with $\Delta M = 1.5$ μ_B f.u.$^{-1}$ Interestingly in the latter two cases, the magnetization of the tetragonal phase is potentially larger than the magnetization in the cubic phase.

The phase diagrams in figure 10 are restricted to Cr_Y since results for Cr_Z only exist for the Co-free system. However, the inclusion of Cr_Z in the homogeneous solution would probably further stabilize the ud^t solution found for Cr_Y and high Co/Cr concentrations. Between averaging over all isomers or using only the most stable isomer, one might also think of different scenarios reflecting the experimental realization of different weights of the atomic positions. For example the assumption of a homogeneous distribution of Cr atoms on the Y-lattice in the cubic phase and an increase of the weight of the $E(c/a)$ branches lowest in energy could be realistic and could result in a transition with $\Delta M \approx 4$ μ_B f.u.$^{-1}$ between cubic uu and tetragonal dd^t phase for small Co concentrations. This magnetization jump would exceed the ones observed in figure 10, however it would require a targeted stabilization of certain atomic orderings.

For $Ni_7Co_1Mn_5Cr_1In_2$ a large change of magnetization between cubic uu and dd^t state has been predicted for a favourable large value of T_E [45] which we cannot find for $Ni_7Co_1Mn_4Cr_1Ga_3$. This prediction was however based only on the one isomer and tetragonal direction with lowest energy, and was thus not representative for the alloy prepared with standard synthesis conditions at high temperatures due to the small energy differences between the atomic orderings. Following the same procedure, we would find a transition from du to dd^t for Co_1 and from uu to dd^t for Co_2 also for our system. In conclusion, both Cr and Co substitution have a large impact on the stability of structural and magnetic phases. Importantly, the details of the atomic distribution thereby outperform small changes in the Mn concentration or the choice of the Z element.

4. Conclusions and outlook

Aiming for compositions which provide a large change of the magnetization (ΔM) at a structural phase transition around ambient temperatures and which are thus promising for magnetocaloric applications, we studied co-doping Cr/Co in Mn-rich Heusler compounds. Promising results have already been reported for this alloy family and it seems natural to replace the expensive In by the isoelectronic more abundant Ga. Therefore, we explored the magnetic structure as well as the transition temperature of its structural phase transition of Ni-Mn-Ga co-doped with Cr/Co, by means of *ab initio* simulations.

Our study based on simulation cells with 16 atoms and different atomic orderings underlines the importance of taking different isomers into account for such a highly frustrated system. Neither the lowest-energy configurations nor the results based on the CPA are representative for the trends found for a homogeneous distribution of atoms, which is more likely for most production processes due to the small energy differences between different isomers. This has to be considered to interpret reported values of transition temperatures and

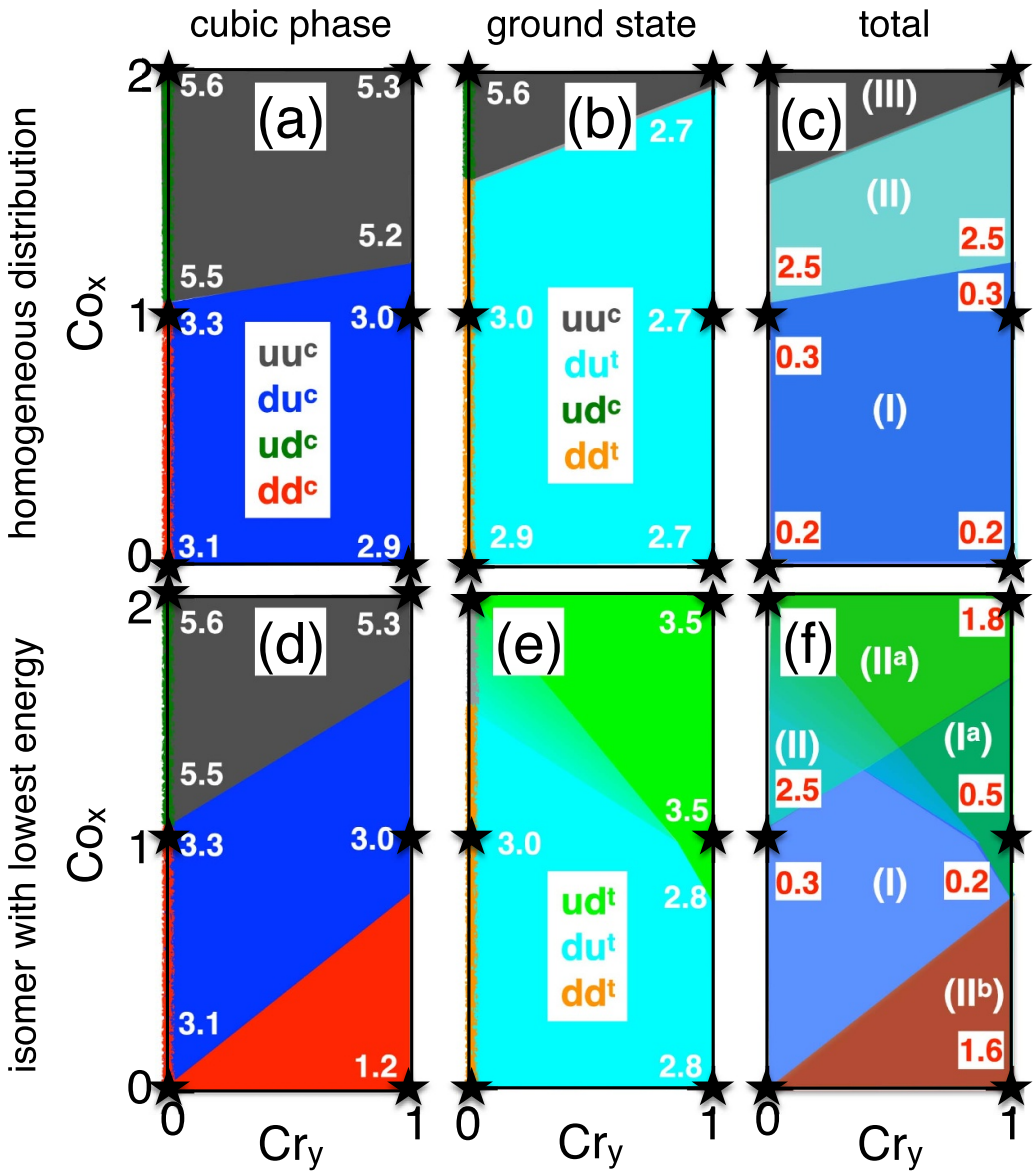

Figure 10. Estimated phase diagrams of $Ni_{8-x}Co_xMn_{5-y}Cr_yGa_3$ for Co on the X lattice and different distribution of Cr atoms on the Y-lattice. Black stars: concentrations realized in our simulations, colours: most stable magnetic phase based on the interpolation in figure 15. Approximate magnetic moments and their change at the structural transition are added in white and red, respectively. Coloured lines: for Cr→0 we cannot distinguish Cr u/d. (a)/(d) Cubic structure, (b)/(e) ground state at $T = 0$ K, and (c)/(f) combined phase diagrams. (a)–(c) homogeneous distribution of Cr on Mn sublattice, (d)–(e) isomer and tetragonal direction lowest in energy. The following different phase sequences can be distinguished: (I): structural phase transition with small change of M: du to du^t or from du to ud^t (I^a), (II) structural phase transition with large change of M, i.e. from uu to du^t or (II^a) from dd to du^t or (II^b) from uu to du^t, and (III): no phase transition.

changes in magnetization based on density functional theory. Furthermore, the strong dependence of magnetic phases and tetragonal minimia on the atomic ordering has important consequences for the interpretation of experimental results: depending on exact process conditions, e.g. quenching rates, the local atomic ordering may be dominated by B2 or by $L2_1$ order . Furthermore, the energetically most favourable isomer may have a higher weight and therefore dominate the systems properties either globally or locally. All scenarios result in different transition temperatures and different magnetic ground states, even for perfect stoichiometry of the sample, a fact which may also contribute to the thermal hysteresis of the transition.

The simple method used here opens also a route to handle complex multicomponent systems, such as high entropy alloys in a similar scheme by using relatively small unit cells and building homogeneous configuration by averaging over many configurations.

For Mn-rich Ni-Mn-Ga we find that both Cr and Co stabilize a full FM alignment of Mn spins and can thus potentially stabilize a large magnetization in the cubic structure. However, both dopants have advantages and disadvantages regarding the tuning of ΔM and T_E. In case of Co, the induced additional FM interactions are rather weak and Co tends to reduce the structural transition temperature T_E. Cr instead imposes large AF interactions which already stabilize the FM alignment of

Mn for low concentrations while introducing frustration into the system. In particular in case of the tetragonal phase, the high level of frustration most likely leads to non-collinear spin structures or at least low T_C for an ordered magnetic phase. In addition, we observe that the frustration of the magnetic system increases with the Cr concentration and for a more quantified understanding it might be illuminating—although beyond the scope of the present paper—to scan the Cr rich region with Monte-Carlo simulations of the Heisenberg model; with magnetic exchange interactions taken from density functional theory simulations to study its magnetic structure in more detail.

In order to narrow down concentration ranges of interest, we have constructed approximate phase diagrams which can serve as a starting point for further systematic simulations in larger simulation cells and experiment. The largest magnetization changes at the phase transition in case of the substitution of Ni by Cr/Co (X lattice) are likely in case of 6% by Cr and 0%–19% by Co. All other concentrations have transitions with a small change of the magnetization or show no phase transition at all. Differently than for $Ni_{7.2}Co_{0.8}Mn_{5.9}In_{2.1}$ with Cr substitution, for which a transition between the uu cubic phase and the du^t or dd^t phases with maximal ΔM has been predicted [43], for the Mn–Ga system, the largest magnetization jump occurs only from uu to du^t (about 2.5 μ_B f.u.$^{-1}$) for the homogeneous distribution of Cr on the Y lattice, whereas no stable dd^t state is observed. Although co-substitution with Co on the X lattice and Cr on the Y lattice reduces the energy of this state relative to the other magnetic phases, the structural phase transition is probably suppressed already for smaller concentrations of dopants. In summary, large changes of the magnetization at the structural phase transition are likely in the co-doped Ni-Mn-Ga system making this material interesting for applications in the predicted concentration ranges. However the maximal change of magnetization between the ordered magnetic phases are smaller than previous reports on In in literature.

Data availability statement

The data that support the findings of this study are available upon reasonable request from the authors.

Acknowledgments

This work was supported by the Deutsche Forschungsgemeinschaft (GR 4792/1-2 and 4792/2). H C H acknowledges support from Vetenkapsrå det, Swedish Foundation for Strategic Research (SSF), eSSENCE, and STandUPP for energy. Calculation resources were provided by the Swedish National Infrastructure for Computing (SNIC) at NSC in Linköping. We acknowledge fruitful discussions with Franziska Scheibel. The authors gratefully thank Peter Entel and Markus E Gruner for inspiring this work.

Appendix A. The role of isomers

In this appendix verbose information on the different isomers and their weighting within the homogenous alloy are summarized. Throughout this work 16-atom simulation cells have been used to describe the different isomers and compositions. These cells allow for only one symmetrically distinct realization of $Ni_8Mn_5Ga_3$, $Ni_7CoMn_5Ga_3$, $Ni_7CrMn_5Ga_3$ and $Ni_8CoMn_4Ga_3Cr_Z$, see figure 11. For two substituents on the X lattice, there are three isomers with different distances between impurities and different spatial orientation of them, see figures 11(d)–(f). For isomer 1, the connection line of both substituents may further be parallel to the tetragonal axis (isomer $1_{||}$, one direction) or perpendicular to the bond (isomer $1_{\perp}$, two possible realizations). For isomer 2, where the two substituents are aligned along $\langle 110 \rangle$, there are three possibilities of choosing the axis, either the bond and the tetragonal axis lie in one plane (isomer $2_{||}$, two realizations) or are perpendicular to each other (isomer $2_{\perp}$). For isomer 3, the two constituents are aligned along $\langle 111 \rangle$ and all three directions are degenerate. For Cr on the Y-lattice, one may distinguish isomer (a) with two Cr_Y-Mn_Z neighbours with a distance of $a/2$ and isomer (b) Cr_Y without direct Mn_Z neighbours and with 8 Ni neighbours with a distance of $\sqrt{3}/2a$ and with Ni in the centre of the connection line, see figures 11(h)–(k). For isomer (a), there is one realization with the connection line parallel to tetragonal axis (isomer $a_{||}$) and two with the tetragonal axis being perpendicular to the bond (isomer $a_{\perp}$). In contrast, the nearest Cr-Mn environment is symmetric with respect to the tetragonal axis for isomer (b).

Differences in energy and magnetization between all (meta-)stable magnetic and structural phases and distinguishable isomers are collected in tables 2 and 3 for Cr on Ni and Cr on Mn or Ga positions, respectively. Full information about the energy depending on the lattice distortion c/a can be found in figure 12 for the case of Cr on Ni and in figure 13 for Cr on the Mn sublattice, respectively. Obviously, for Cr on the Ni sublattice most isomers follow the same trends. The only exception is observed in case of 2 Cr atoms ($x_1 = 2, x + 2 = 0$); where a larger spread of the energy differences occurs, see figure 12(b). For Cr on Mn sites, the spread of $E(c/a)$ curves of the different isomers is bigger, but also here, a clear preference of tetragonal distortions is present, see figure 13.

Appendix B. Energies for homogeneous distribution of atoms

Assuming a uniform probability for the atoms to occupy different positions within one sublattice, the mean energy for each case can be calculated from the energies if the different isomers are weighted with their possible realizations in our

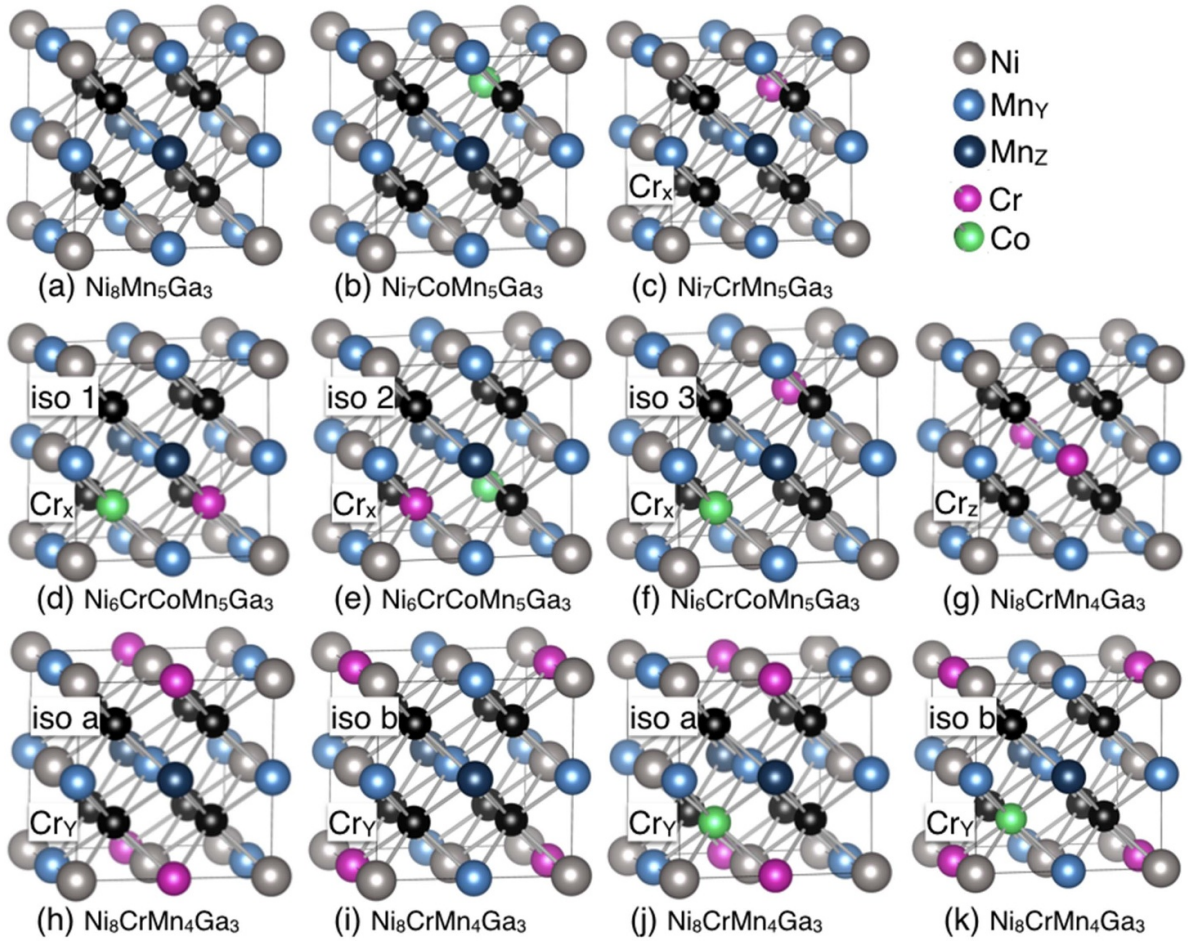

Figure 11. Collection of different distinguishable atomic structures for a given stoichiometry and sublattice occupation. (a) initial structure without doping (b)–(f) substitution on Ni lattice (X), for (b)–(c) substitution of single Co and Cr atoms and (d)–(f) for the three possible isomers for two substituents exemplary shown for substitution with Cr and Co. (g) Single realization of Cr on Ga lattice (Z), (h)–(k) Cr on Mn, i.e. Y lattice for isomers (a) and (b) with additional substitution of Co on Ni in the latter cases.

Table 2. Collection of magnetic moments (M) and energy differences between magnetic states and structural phases for all isomers of $Ni_{8-x-y}Cr_xCo_yMn_5Ga_3$. Energies are given relative to the state with the highest moment at $c/a = 1$ and are also converted to an approximate transition temperature, T_E. Indices t refer to tetragonal structures and for isomers with two relative alignments between the characteristic bond and the tetragonal axis, first the values for perpendicular orientation are given.

		a (Å)	c/a	ΔE (meV f.u.$^{-1}$)	ΔE_t	T_E (K)	M (μ_B f.u.$^{-1}$)	M_t
				$Ni_8Mn_5Ga_3$				
	u	5.826	1.22	0	−27		5.3	5.2
	d	5.814	1.30	−22	−97	218	3.1	2.9
				$Ni_7CoMn_5Ga_3$				
	u	5.817	—	0	—		5.5	—
	d	5.805	1.26	−1	−34	96	3.3	3.0
				$Ni_7CrMn_5Ga_3$				
	ud	5.822	1.24	0	−16	46	4.5	4.2
	dd	5.809	1.30	50	−2		2.2	2.0
				$Ni_6CoCrMn_5Ga_3$				
isomer1	ud	5.815	—/1.04	0	—/−3	—/ 9	4.6	—/4.6
	dd	5.802	1.28/1.04	68	59/68	—	2.3	1.9/1.9
isomer2	ud	5.816	—/—	0	—/—	—	4.6	—/—
	dd	5.803	1.26/1.28	71	63/46	—	2.4	2.0/1.0
isomer3	ud	5.816	—	0	—	—	4.6	—
	dd	5.803	1.28	77	45	—	2.4	1.9
				$Ni_6Co_2Mn_5Ga_3$				
isomer1	u	5.798	—/1.04	0	—/-5	—/14	5.5	—/5.5
	d	5.786	1.22/1.10	21	27/14	—/—	3.4	3.2/3.3
isomer2	u	5.800	—/—	0	—/—	—/—	5.6	—/—
	d	5.788	1.22/1.22	20	18/19	—/—	3.4	3.2/3.1
isomer3	u	5.800	—	0	—	—/—	5.6	—
	d	5.788	1.22	23	21	—/—	3.4	3.1
				$Ni_6Cr_2Mn_5Ga_3$				
isomer1	ud	5.829	—/1.22	0	—/−18	—/52	3.6	—/3.1
	dd	5.816	1.26/1.30	83	112/ 47	—	1.5	1.3/1.0
isomer2	ud	5.830	1.30/1.22	0	−45/−2	131/6	3.6	2.8/3.2
	dd	5.814	1.30/1.34	101	76/31	—	1.7	1.2/1.0
isomer3	ud	5.834	1.30	0	−29	84	3.4	2.7
	dd	5.812	1.32	94	32	—	1.8	1.3

Table 3. Collection of magnetic moments (M) and energy differences between magnetic states and structural phases for all isomers of $Ni_{8-y}Co_yMn_{5-x}Cr_xGa_3$. Energies are also converted to an approximate transition temperature, T_E. Indices t refer to tetragonal structures and for isomers with two relative alignments between the characteristic bond and the tetragonal axis, first the values for perpendicular direction are given.

		a (Å)	c/a	ΔE	ΔE_t (meV f.u.$^{-1}$)	T_E (K)	M	M_t (μ_B f.u.$^{-1}$)
				$Ni_8Mn_4CrGa_3$				
isomer a	uu	5.825	1.22/1.24	0	−29/−28	—/—	5.1	5.0/5.0
	ud	5.823	1.26/—	−28	−114/—	206/—	3.4	3.4/—
	du	5.816	1.30/1.30	−43	−137/−95	273/150	3.0	2.8/2.7
	dd	5.817	1.28/1.30	−13	−33/−118	—/218	1.2	1.4/1.2
isomer b	uu	5.826	1.24	0	−25	—	5.1	5.0
	ud	5.828	1.22	46	13	—	3.4	3.4
	du	5.814	1.30	31	−49	6	2.7	2.6
	dd	5.816	1.28	−47	−78	90	1.1	1.0
Cr on Ga	u	5.819	1.24	0	−32	—	5.0	4.9
	d	5.806	1.32	−57	−162	305	3.2	3.1
				$Ni_7CoMn_4CrGa_3$				
isomer a	uu	5.816	—/1.18	0	—/ 17	—/—	5.2	–/5.0
	ud	5.815	1.24/—	−11	−75/—	160/—	3.6	3.5/—
	du	5.807	1.28/1.26	−20	−67/−36	136/46	3.1	2.8/2.7
	dd	5.808	1.26/1.30	30	5/−85	− /189	1.4	1.4/1.1
isomer b	uu	5.817	—	0	—	—	5.2	—
	ud	5.820	1.22	59	51	—	3.6	3.4
	du	5.805	1.28	46	5	—	2.8	2.6
	dd	5.809	1.28	−9	−52	125	1.3	1.1
				$Ni_6Co_2Mn_4CrGa_3$				
isomer a	uu	5.798	—/—	0	—/—		5.3	—/—
	ud	5.798	1.24/—	5	−48/—	139/—	3.7	3.5/—
	du	5.789	1.26/1.24	7	−15/6	44/—	3.2	2.8/2.7
	dd	5.790	1.26/1.28	68	45/−50	—/145	1.7	1.5/1.2
isomer b	uu	5.799	—	0	—	—	5.4	—
	ud	5.803	—	63	—	—	3.9	—
	du	5.787	1.26	64	42	—	3.0	2.5
	dd	5.792	1.26	27	−19	55	1.6	1.2

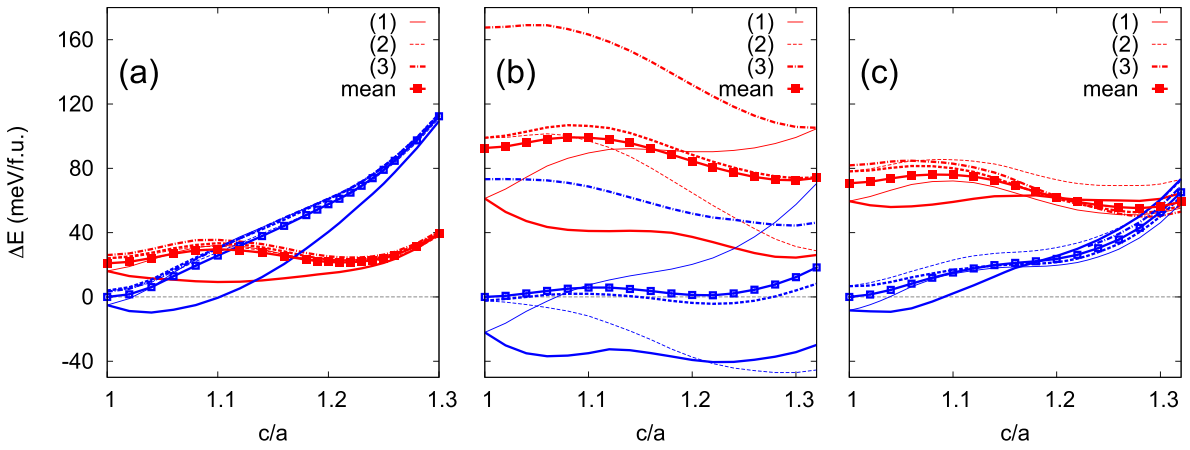

Figure 12. Energy variation with tetragonal distortion of $Ni_{8-x_1-x_2}Cr_{x_1}Co_{x_2}Mn_5Ga_3$. Blue and red lines correspond to Mn_Z u and d respectively, and the energy is given relative to the u state for $c/a = 1$. Cr and Co are aligned d and u, respectively. Different isomers and directions of the tetragonal distortion (solid lines: isomer 1, dashed lines: isomer 2, dashed dotted lines: isomer 3; Thin lines: tetragonal axis perpendicular to x_i-x_j bond, thick lines: 1, 2, 3 components of x_i-x_j bond parallel to c/a for isomers 3, 2, 1. Lines with points: averaged curve for a uniform distribution of atoms.) (a) $x_1 = 0, x_2 = 2$, i.e. Co. (b) $x_1 = 2, x_2 = 0$, i.e. Cr. (c) $x_1 = 1 = x_2$.

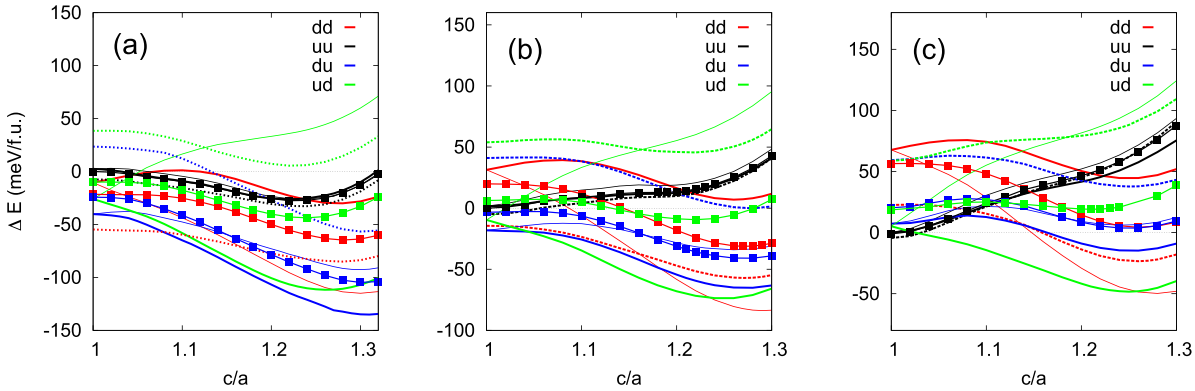

Figure 13. Impact of Co_X on the energy variation with tetragonal distortion for $Ni_{8-x_1}Co_{x_1}Mn_4CrGa_3$ for Cr on the Mn lattice (Cr_Y). (a) $x_1 = 0$ (b) $x_1 = 1$ (c) $x_1 = 2$; Solid lines: isomer 1, dashed lines: isomer 2, thick lines: tetragonal axis perpendicular to Cr-Mn_Z bond, thin lines: tetragonal axis and Cr-Mn_Z bond parallel to each other; lines with symbols: mean values. Note: for (c) we only considered the Co-Co distribution with highest symmetry (isomer 3).

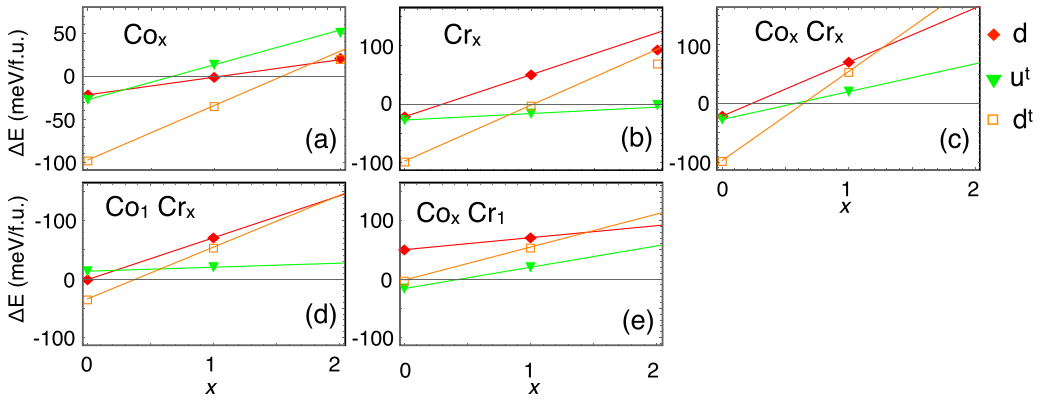

Figure 14. Construction of phase diagrams in dependency of the concentration of Cr and Co on the Ni sublattice. All energies are given relative to the cubic FM state (a) Co_x with $Cr_x = 0$; (b) Cr_x with $Co_x = 0$; (c) Cr_x and Co_x; (d) Cr_x with $Co_x = 1$; (e) Co_x with $Cr_x = 1$. The intersections of these figures are used to determine the phase boundaries in figure 9.

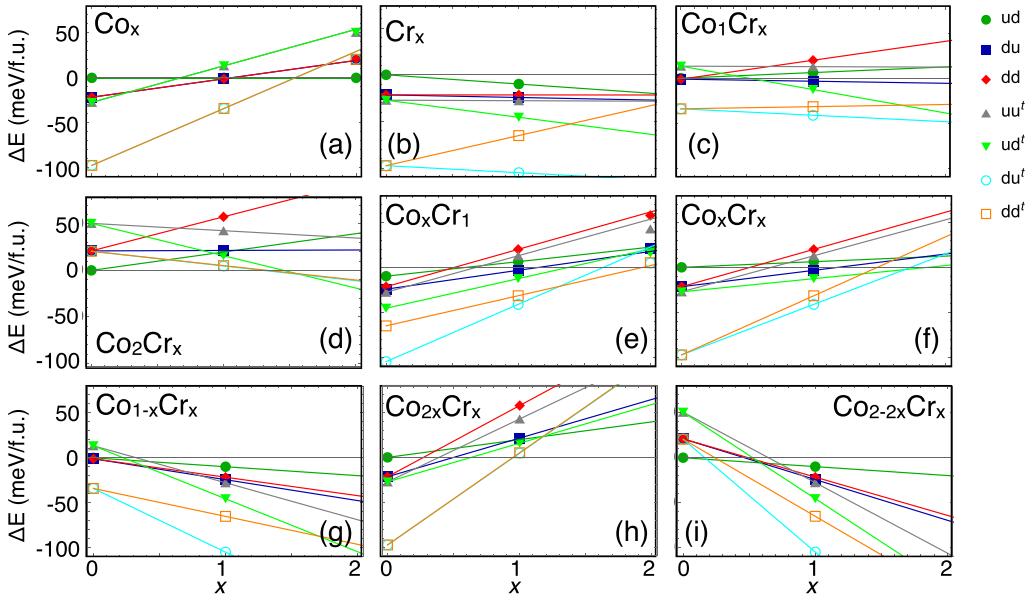

Figure 15. Construction of phase diagrams: energies for Co_x substituted for Ni and Cr_x substituted for Mn_Y atoms relative to cubic uu state. The intersections are used for the construction of the approximate phase diagram in figure 10.

Table 4. Impact of the choice of the exchange-correlation potential on magnetic moments in μ_B f.u.$^{-1}$ as found in KKR-CPA simulations for du phase of $Ni_7CoMn_4CrGa_3$ and ud phase of $Ni_6CoCrMn_5Ga_3$.

$Ni_7CoMn_4CrGa_3$	Ni	Mn_Y	Mn_Z	Co	Cr
GGA	0.19	3.99	−4.13	0.77	3.46
LDA	0.21	3.86	−3.95	0.63	3.25
$Ni_6CoCrMn_5Ga_3$					
GGA	0.49	3.38	3.45	1.16	−2.13
LDA	0.49	3.21	3.30	1.15	−1.18

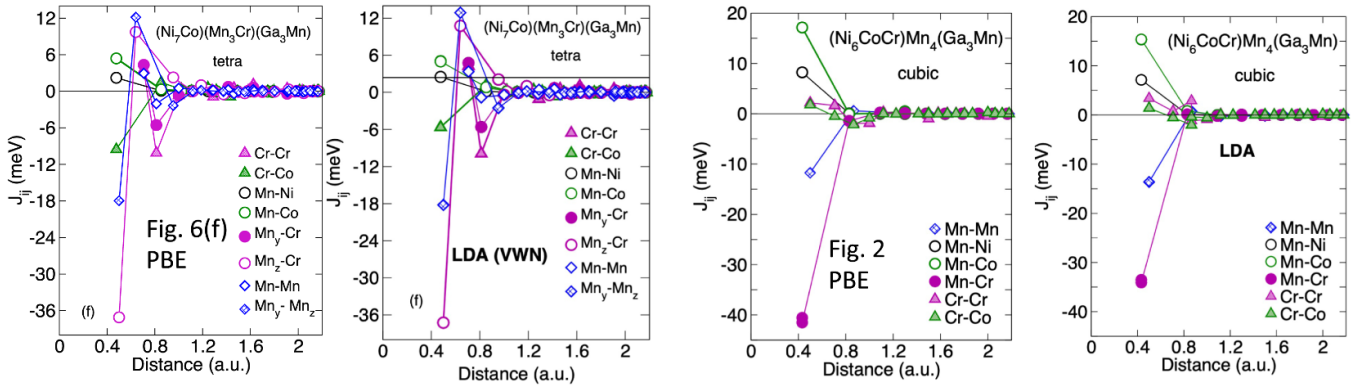

Figure 16. Robustness of magnetic exchange parameters to the choice of the exchange-correlation potential. Results obtained by PBE ((a), (c)) are compared to results obtained by LDA ((b), (d)) for the examples ((a), (d)) Ni_7CoMn_4CrGa and ((b), (d)) $Ni_6CoCrMn_5Ga_3$.

cell. The expression for averaging the energy for two substituents on the X lattice is then:

$$E_{\text{mean}} = (E_{1,||} + 2 * E_{1,\perp} + E_{2,\perp} + 2 * E_{2,||} + E_3)/7\,. \quad (1)$$

and for Cr on Mn:

$$E_{\text{mean}} = (E_{a,||} + 2 * E_{a,\perp} + E_b)/4\,. \quad (2)$$

One may also consider the homogeneous distribution of Cr on Y and Z lattice. Keeping the stoichiometry of Ni_8Mn_4CrGa, the mean energy in this case amounts to:

$$E_{\text{mean}} = (E_{a,||} + 2 * E_{a\perp} + E_b + 4E_Z)/8, \quad (3)$$

with E_Z the energy of the configuration with Cr on one of the four degenerated Ga positions.

Finally, figures 14 and 15 illustrate in more detail how the phase diagrams have been constructed. First, we plot the energy differences of all magnetic states for cubic and tetragonal phases relative to the cubic uu (or if not stable ud) state in dependency of Cr and Co concentrations. Hereby, the mean energies of all relevant isomers are used and if the tetragonal phase is no longer stable, we instead use the energy of the remanent extrema of higher order. Second, linear interpolation between the data points for $x = 0$ and $x = 1$ is used for an approximate determination of stability ranges. The crossings of the interpolations are used to assign the stability ranges of the different magnetic states for the cubic structure and the energetic ground state at 0 K.

For Co substitution on the X lattice, we find that if three data points exist they are following this linear trend. For Cr on the X sublattice, the energy difference is not fully linear for d and d^t. The deviations of the data points for $x = 2$ from the linear fit (made from data for $x = 0$ and 1) are about 25 meV f.u.$^{-1}$ However, this has minor influence on the results and no change in the order of the phases is observed.

Appendix C. Magnetic background

In our manuscript we assume that the spins in Ni, Mn_Y and Co sublattices always align parallel to each other. This assumption is justified by the FM exchange interactions between Mn_Y and Co or Ni. We furthermore tested different alignments of the sublattice magnetization in random samples and systematically for all isomers of $Ni_6CoCrMn_5Ga_3$ in the cubic and tetragonal structures. In all these cases, the configuration with antiparallel Mn_Y and Co or Ni magnetization are not stable already during static simulations at $T = 0$ K and result in one of magnetic structures included in our manuscript.

Appendix D. Magnetic exchange interactions

To demonstrate the effect of the exchange correlation potential on the magnetic properties, we compare our CPA-KKR results obtained by PBE to calculations using the Vosko-Wilk-Nussair functional [76]. As examples, table 4 and figure 16 compare the obtained magnetic moments and J_{ij} for $Ni_7CoMn_4CrGa_3$ and $Ni_6CoCrMn_5Ga_3$. As expected, the moments in GGA are slightly larger compared to ones obtained by LDA. The biggest change is observed for Cr in $(Ni_6CoCr)Mn_5Ga_3$. In this case the moment is 15% smaller in LDA simulations. The

J_{ij} values follow this trend. While for Cr on Y, hardly any change can be observed; small changes are visible in the Cr on X case (right hand side) in figure 16. Also, here the largest changes occur for the Cr couplings. However, none of the changes alters the observed trends or would lead to different conclusions.

ORCID iDs

H C Herper https://orcid.org/0000-0001-6159-1244
A Grünebohm https://orcid.org/0000-0001-9299-058X

References

[1] Çakır A, Righi L, Albertini F, Acet M, Farle M and Aktürk S 2013 *J. Appl. Phys.* **114** 183912
[2] Cong D Y, Roth S and Schultz L 2012 *Acta Mater.* **60** 5335
[3] Grünebohm A, Herper H C and Entel P 2016 *J. Phys. D: Appl. Phys.* **49** 395001
[4] Felser C, Wollmann L, Chadov S, Fecher G H and Parkin S S P 2015 *APL Mater.* **3** 041518
[5] Dutta B, Çakır A, Giacobbe C, Al-Zubi A, Hickel T, Acet M and Neugebauer J 2016 *Phys. Rev. Lett.* **116** 025503
[6] Krenke T, Acet M, Wassermann E F, Moya X, Mañosa L and Planes A 2005 *Phys. Rev.* B **72** 014412
[7] Waske A, Dzekan D, Sellschopp K, Berger D, Stork A, Nielsch K and Fähler S 2019 *Nat. Energy* **4** 68
[8] Herper H C and Grünebohm A 2018 *IEEE Trans. Magn.* **55** 2100804
[9] Caron L *et al* 2017 *Phys. Rev.* B **96** 054105
[10] Planes A, Mañosa L and Acet M 2009 Magnetocaloric effect and its relation to shape-memory properties in ferromagnetic Heusler alloys *J. Phys.: Condens. Matter* **21** 233201
[11] Graf T, Felser C and Parkin S S P 2011 *Prog. Solid State Chem.* **39** 1
[12] Zhang X 2018 *Chin. Phys.* B **27** 127101
[13] Miracle D 2019 *Nat. Commun.* **10** 1805
[14] Walsh F, Asta M and Ritchie R O 2021 *Proc. Natl Acad. Sci. USA* **118** e2020540118
[15] Entel P, Siewert M, Gruner M E, Chakrabarti A, Barman S R, Sokolovskiy V V and Buchelnikov V D 2013 *J. All. Comp.* **577** S107
[16] Uijttewaal M A, Hickel T, Neugebauer J, Gruner M E and Entel P 2009 *Phys. Rev. Lett.* **102** 035702
[17] Siewert M *et al* 2012 *Adv. Eng. Mater.* **14** 530
[18] Siewert M *et al* 2011 *Appl. Phys. Lett.* **99** 191904
[19] Sokolovskiy V V, Buchelnikov V D, Zagrebin M A, Entel P, Sahoo S and Ogura M 2014 *Entropy* **16** 4992
[20] Grünebohm A, Comtesse D, Hucht A, Gruner M E, Maskovskaya A and Entel P 2014 *IEEE Trans. Magn.* **50** 2506004
[21] Umetsu R Y, Sheikh A, Ito W, Ouladdiaf B, Ziebeck K R A, Kanomata T and Kainuma R 2011 *Appl. Phys. Lett.* **98** 042507
[22] Sokolovskiy V V, Grünebohm A, Buchelnikov V D and Entel P 2014 *Entropy* **16** 4992
[23] Fabbrici S *et al* 2011 *Acta Mat.* **59** 412
[24] Segui C and Cesari E 2012 *J. Appl. Phys.* **111** 043914
[25] Dutta B, Körmann F, Hickel T and Neugebauer J 2018 *Phys. Status Solidi* b **255** 1700455
[26] Sharma V K, Chattopadhyay M K, Chandra L S S and Roy S B 2011 *J. Phys. D: Appl. Phys.* **44** 145002
[27] Khan M, Brock J and Sugerman I 2016 *Phys. Rev.* B **93** 054419
[28] Adachi Y, Kouta R, Fujio M, Kanomata T, Umetsu R Y, Xu X and Kainuma R 2015 *Phys. Proc.* **75** 1187
[29] Khan M *et al* 2012 *Appl. Phys. Lett.* **100** 172403
[30] Kök M, Durgun S B and Ozen E 2019 *J. Therm. Anal. Calorim.* **136** 1147–52
[31] Schleicher B *et al* 2017 *J. Phys. D: Appl. Phys.* **50** 465005
[32] Zagrebin M A, Sokolovskiy V V and Buchelnikov V D 2017 *Intermetallics* **87** 55–60
[33] Zhang Y, Kumar S V, Xiang W, Wu Z and Sun Z 2021 *Mater. Sci. Eng.* A **804** 140777
[34] Umetsu R Y, Saito K, Ono K, Fukushima T, Kuroda F, Oguchi T and Ishigaki T 2021 *J. Alloy. Compd.* **855** 157389
[35] Kumar A S, Ramudu M and Seshubai V 2021 *J. Supercond. Nov. Magn.* **34** 479–87
[36] Sánchez-Alarcos V, Recarte V, Pérez-Landazábal J I, Chapelon J R and Rodríguez-Velamazán J A 2011 *J. Phys. D: Appl. Phys.* **44** 395001
[37] Río-López N A, Lázpita P, Salazar D, Petrenko V I, Plazaola F, Chernenko V and Porro J M 2021 *Metals* **11** 829
[38] Entel P, Gruner M E, Acet M, Çakır A, Arróyave R, Duong T, Sahoo S, Fähler S and Sokolovskiy V V 2018 *Energy Technol.* **6** 1478–90
[39] Şaşmaz M, Dreist F, Iglesias I, Çakır A, Farle M and Acet M 2020 *Phys. Rev.* B **102** 064401
[40] Çakır A, Koyun H N, Acet M and Farle M 2020 *J. Magn. Magn. Mater.* **499** 166265
[41] Comtesse D *et al* 2014 *Phys. Rev.* B **89** 184403
[42] Pathak A K, Dubenko I, Xiong Y, Adams P W, Stadler S and Ali N 2011 *J. Appl. Phys.* **109** 07A916
[43] Sokolovskiy V V, Buchelnikov V D, Gruner M E and Entel P 2015 *IEEE Trans. Magn.* **51** 2502504
[44] Sharma V K, Chattopadhyay M K and Roy S B 2010 *J. Phys. D: Appl. Phys.* **43** 225001
[45] Sokolovskiy V V, Entel P, Buchelnikov V D and Gruner M E 2015 *Phys. Rev.* B **91** 220409
[46] Buchelnikov V D, Sokolovskiy V V, Miroshkina O N, Baigutlin D R and Zagrebin M A 2020 *Phys. Metals Metallogr.* **121** 202–9
[47] Czaja P, Chulist R, Zywczak A, Hawelek L and Przewoznik J 2017 *Magnetochemistry* **3** 24
[48] 2005 Rare earth elements—critical resources for high technology (Available at: http://pubs.usgs.gov/fs/2002/fs087-02/)
[49] 2020 Prices of chemical elements (Available at: https://en.wikipedia.org/wiki/Prices_of_chemical_elements)
[50] Orlandi F, Fabbrici S, Albertini F, Manuel P, Khalyavin D D and Righi L 2016 *Phys. Rev.* B **94** 140409
[51] Orlandi F, Çakır A, Manuel P, Khalyavin D D, Acet M and Righi L 2020 *Phys. Rev.* B **101** 094105
[52] Zagrebin M A, Sokolovskiy V V and Buchelnikov V D 2019 *J. Magn. Magn. Mater.* **470** 123
[53] Zagrebin M A, Sokolovskiy V V, Smolyakova E E and Buchelnikov V D 2017 *Mater. Res. Express* **4** 026105
[54] We note that we also tested different initial alignments of Ni and Co spins relative to the Mn_Y background. However, these spin configurations turned out to be unstable already during static DFT simulations, see details for the example of $Ni_6CoCrMn_5Ga_3$ in the appendix.
[55] Kresse G and Furthmüller J 1996 *Phys. Rev.* B **54** 11169
[56] Blöchl P E 1994 *Phys. Rev.* B **50** 17953
[57] We note that it is commonly accepted that the inclusion of 3p electrons for the 3d elements may be important for elements up to Mn, while it influences the structural and magnetic properties for Co and Ni only weakly. Therefore, it is always a compromise between saving computational time and increasing the accuracy of the results. Due to historical reasons we made different choices for Co and Ni. Simulations with the 3p electrons of Co treated as valence

electrons do not show any significant changes of the results. For the randomly chosen test cases $Ni_6CrCoMn_5Ga_3$ (isomer 1, tetragonal, and isomer 3, cubic) the changes of magnetic moments and energy differences between ud and dd states are not exceeding $0.01\mu_B$/atom and 0.5 meV f.u.$^{-1}$, respectively, which is far too small to alter the observed trends.

[58] Perdew J P, Burke K and Ernzerhof M 1996 *Phys. Rev. Lett.* **77** 3865

[59] Blöchl P E, Jepsen O and Andersen O K 1994 *Phys. Rev.* B **49** 16223

[60] Monkhorst H J and Pack J D 1976 *Phys. Rev.* B **13** 5188

[61] We note that relaxation of volume and atomic positions would reduce the energy of the tetragonal phases. For the randomly picked test case Ni_7CrMn_5Ga we find a reduction by 0.1 meV f.u.$^{-1}$ for the relaxation of volume and of 5 and 18 meV f.u.$^{-1}$ for the optimization of the ionic positions. These changes do not justify time-consuming full relaxation as the estimate of the transition temperatures anyway have an error bar of about 50 K [15] and the qualitative phase diagrams are not modified.

[62] Liechtenstein A I, Katsnelson M I, Antropov V P and Gubanov V A 1987 *J. Magn. Magn. Mater.* **67** 65

[63] The Munich SPR-KKR package, version 3.6 Ebert H *et al* 1986 Fully relativistic band structure calculations for magnetic solids—formalism and application *Electronic Structure and Physical Properties of Solids (Lecture Notes in Physics)* vol 535, ed H Dreyssé (Berlin: Springer) p 191

[64] Ebert H 1996 *Rep. Prog. Phys.* **59** 1665

[65] Gonz'alez-Legarreta L, Caballero-Flores R, Rosa W O, Ipatov M, Escoda L, Sunõl J, Prida V, Gonz'alez J and Hernando B 2016 *Heusler Alloy Ribbons: Structure, Martensitic Transformation, Magnetic Transitions and Exchange Bias Effect (Springer Series in Materials Science)* vol 231 (Berlin: Springer)

[66] Entel P *et al* 2013 *Eur. Phys. J.* B **86** 65

[67] Madiligama A, Ari-Gur P, Shavrov V, Koledov V, Ren Y, Calder S and Kayani A 2015 *Effects of Cobalt on the Crystalline Structures of the Ni-Mn-In Giant Magnetocaloric Heusler Alloys (Springer Proc. in Energy)* (Berlin: Springer)

[68] He W Q, Huang H B, Liu Z and Ma X 2017 *Intermetallics* **90** 140

[69] Pandey S *et al* 2017 *AIP Adv.* **7** 056433

[70] Entel P, Gruner M E, Comtesse D, Sokolovskiy V V and Buchelnikov V D 2014 *Phys. Status Solidi* b **251** 2135

[71] We note that there is an exception for Cr-rich systems ($x_2 = 2$) in which the differences between isomers can reach 100 meV f.u.$^{-1}$ However the weight of such outliers is small as shown in figure 3(a) for $x_1 = 1, x_2 = 1$, i.e. $Ni_6CrCoMn_5Ga_3$.

[72] Entel P *et al* 2015 *MATEC Web Conf.* **33** 02001

[73] In contrast to the findings for Ni substitution the Cr u solutions can be stabilized as the AF Cr-Mn interaction is reduced from about -40 meV f.u.$^{-1}$ to about -16 meV f.u.$^{-1}$

[74] Note in case of isomer (a) the average of the two possible tetragonal configurations has been used to determine T_E while in case of isomer (b) only one tetragonal solution exists.

[75] We note that we assume that the tetragonal system is within one magnetic phase. If we lift this condition, an slightly larger energy difference T_E was possible assuming a mixture of ud and uu phases, see table 3.

[76] Vosko S H, Wilk L and Nusair M 1980 *Can. J. Phys.* **58** 1200–11